REPORT DOCUMENTATION PAGE

1. REPORT DATE (DD-MM-YYYY)	2. REPORT TYPE	3. DATES COVERED (From - To)
01-12-2005	Interim Report	August 2003-December 2005

4. TITLE AND SUBTITLE

Characteristics of the Contraction of the Boeing/AFOSR Mach-6 Quiet Tunnel

5a. CONTRACT NUMBER

5b. GRANT NUMBER

F49620-03-1-0030

5c. PROGRAM ELEMENT NUMBER

6. AUTHOR(S)

Matthew P. Borg

5d. PROJECT NUMBER

5e. TASK NUMBER

5f. WORK UNIT NUMBER

7. PERFORMING ORGANIZATION NAME(S) AND ADDRESS(ES)

Purdue University, School of Aeronautics and Astronautics

8. PERFORMING ORGANIZATION REPORT NUMBER

9. SPONSORING/MONITORING AGENCY NAME(S) AND ADDRESS(ES)

Air Force Office of Scientific Research, Dr. John Schmisseur
875 North Randolph Street
Suite 325, Room 3112
Arlington, VA 22203

10. SPONSOR/MONITOR'S ACRONYM(S)

AFOSR

11. SPONSOR/MONITOR'S REPORT NUMBER(S)

12. DISTRIBUTION/AVAILABILITY STATEMENT

Approved for public release. Distribution unlimited.

13. SUPPLEMENTARY NOTES

M.S. Thesis documenting performance of national research facility.

14. ABSTRACT

The Boeing/AFOSR Mach-6 Quiet Tunnel continues to be developed to simulate the low noise of the free-flight environment. An investigation of the flow entering the contraction of this facility was necessary to determine whether disturbances in the driver tube are of sufficient amplitude to propagate downstream into the test section of the tunnel. Significant free convection was found in the nominally stagnant pre-run air of the contraction and leads to significant stratification of the air in the driver tube during the run. Two calibration methods were tested and used to compute mass-flow fluctuations in the contraction at a variety of locations and pressures. For regions near the center of the contraction, mass-flow fluctuations of 1.4% were marginally higher than Beckwith's allowable criterion of 1% for settling-chamber noise. This may not preclude quiet flow to the design conditions, since an aluminum surrogate nozzle recently provided quiet flow to 94 psia, 2/3 of the design performance.

15. SUBJECT TERMS

hypersonic laminar-turbulent transition, quiet wind tunnels, freestream noise and turbulence

16. SECURITY CLASSIFICATION OF:			17. LIMITATION OF ABSTRACT	18. NUMBER OF PAGES	19a. NAME OF RESPONSIBLE PERSON
a. REPORT	b. ABSTRACT	c. THIS PAGE	Unlimited	105	Steven P. Schneider, Professor
U	U	U			19b. TELEPHONE NUMBER (Include area code) 765-494-3343

CHARACTERISTICS OF THE CONTRACTION OF THE BOEING/AFOSR

MACH-6 QUIET TUNNEL

A Thesis

Submitted to the Faculty

of

Purdue University

by

Matthew P. Borg

In Partial Fulfillment of the

Requirements for the Degree

of

Master of Science

December 2005

ACKNOWLEDGMENTS

First and foremost, I thank my Lord and Savior, Jesus Christ, without whom I could never have done this. He daily provides strength and grace to get through it all.

I also thank my advisor, Steve Schneider for all of his time, help, suggestions, and for finding the funds that allow me to be in grad school. Thanks also to Steve Collicott and Dave Kuntz for serving on my committee (and passing me) and providing helpful insights.

Without the help of many people at the ASL, I could not have completed this research. Many thanks to Madeline Chadwell, Jim Younts, Robin Snodgrass, and Jerry Hahn for all the help and the great care you've taken to machine quality parts and maintain the lab. Thanks also to Joan Jackson for taking care of all my office needs and for providing some entertainment from time to time.

My great appreciation and thanks also goes out to my family. Thanks dad, mom, Michael, and Kyle for all of your love and support throughout my whole life and in these past two years as I've sought this degree. Even though you haven't understood everything I've done, you've still been interested and tried to understand. You mean so much to me. I love you all.

And where would I be without my fellow laborers in research? Shann Rufer, Craig Skoch, Erick Swanson, Justin Smith (smith543), Tom Juliano, and Tyler Robarge, thank you all for your support, friendship, and help in solving the problems that are unavoidable in this field. And even if you haven't appreciated them as much as you should have, thanks for putting up with my nerdiness, bad jokes, and aberrant behavior (i.e. hyperactivity) after having ingested *way* too much caffeine.

Will Strattner and Aaron Mullins, thanks for being such great roommates and friends. Thanks for all the support and for putting up with me, even when I wasn't the most pleasant of people because of school and research. And thanks for helping me to seek the LORD, relax and have some fun along the way too. You guys are a blessing.

Soli Deo Gloria!

TABLE OF CONTENTS

LIST OF TABLES

LIST OF FIGURES

NOMENCLATURE

A^*	Nozzle-throat area
A_c	Contraction cross-section area
A	Calibration constant
a	Calibration constant
B	Calibration constant
b	Calibration constant
C	Calibration constant
d	Hot-wire diameter
E	Hot-wire voltage
g	Acceleration due to gravity
Gr	Grashof number
k	Thermal conductivity
l	Hot-wire length
$\dot{m}$	Mass flow rate
M	Mach number
Nu	Nusselt number
n	Calibration constant
P	Pressure
R	Resistance
R_a	Arm resistance in constant temperature anemometer
R^2	Correlation Coefficient
Re	Reynolds Number
t	Time
T	Temperature
U	Contraction-air velocity

y_t	Distance below upper contraction wall
y_c	Distance from contraction centerline
z	Axial distance from the geometric throat
Δt	Time step used in calibration
Δt_{mff}	Time step used in fluctuation calculations
V	Driver-tube volume
β	Coefficient of expansion
γ	Ratio of specific heats
η	Recovery factor
μ	Kinematic viscosity
ν	Dynamic viscosity
ρ	Density
σ	Ratio of density to sea-level density

Subscripts

f	Film conditions
i	Initial conditions
0	Stagnation conditions
w	Wire conditions

ABSTRACT

Borg, Matthew P. M.S., Purdue University, December, 2005. Characteristics of the Contraction of the Boeing/AFOSR Mach-6 Quiet Tunnel. Major Professor: Steven P. Schneider.

The Boeing/AFOSR Mach-6 Quiet Tunnel continues to be developed to simulate the low noise of the free-flight environment. An investigation of the flow entering the contraction of this facility was necessary to determine whether disturbances in the driver tube are of sufficient amplitude to propagate downstream into the test section of the tunnel. Significant free convection was found in the nominally stagnant pre-run air of the contraction and leads to significant stratification of the air in the driver tube prior to a run. The non-uniform temperatures in the contraction due to both axial and radial wall-temperature gradients are thought to be the cause. Additionally, thick thermal and viscous boundary layers were found to be present along the top contraction wall during tunnel runs. If such boundary layers exist on the lower contraction wall, they were not detected and must thus be thinner. Two calibration methods were tested and used to compute mass-flow fluctuations in the contraction at a variety of locations and pressures. For distances y_c = -6.00 to 3.00 inches, the mass-flow fluctuations of 1.4% were marginally higher than Beckwith's criterion of 1% for allowable settling-chamber noise. At 6.00 inches, they were found to be significantly higher at 2.5%. However, since the BAM6QT has a much larger contraction ratio than Beckwith's tunnels, more of the noise may be reflected back into the driver tube. This may not preclude quiet flow since an aluminum surrogate nozzle-throat recently provided quiet flow to 94 psia.

1. Introduction

1.1   The Need for Hypersonic Facilities

The stability and transition of hypersonic boundary layers have many ramifications for vehicles flying at hypersonic velocities for extended periods of time. Many variables such as drag, control forces, and heat transfer are affected by the state of the boundary layer. The many mechanisms leading to transition are still poorly understood, thus rendering boundary-layer in-flight prediction difficult and uncertain.

In order to obtain experimental data that are useful for prediction of boundary-layer instability and transition for a flight vehicle, conditions must be close to those of the flight environment. This situation is especially difficult to realize in the laboratory environment due to the high levels of noise radiated from the normally-turbulent boundary layers on conventional wind tunnel walls and the lack of chemistry effects that are present in flight. Most traditional wind tunnels have free stream noise levels of 0.5-1.0%, two orders of magnitude higher than those experienced in flight [1,2]. It has been demonstrated that this increased noise level can lead to early transition or bypass normal transition mechanisms entirely [3], making efforts to predict in-flight transition to be unreliable at best.

Hypersonic wind tunnels having low noise levels are essential to better understand transition on hypersonic vehicles. Such facilities would enable much more accurate predictions of boundary layer stability and transition for full-size hypersonic vehicles.

1.2 The BAM6QT

1.2.1 The Tunnel

To this end, a quiet hypersonic facility was constructed at Purdue University. The tunnel is designed to operate at Mach 6 and have laminar boundary layers up to a throat unit Reynolds number of 10^8/m, which corresponds to a stagnation pressure of approximately 150 psia [4]. Quiet flow requires free stream RMS fluctuations of less than about 0.1%.

The Purdue facility, a schematic of which can be seen in Figure 1.1, was designed as a Ludwieg tube. A Ludwieg tube consists of a long driver tube followed by a converging-diverging nozzle, second throat, diffuser, and large vacuum chamber. In the case of the Boeing/AFOSR Mach-6 Quiet-Tunnel (BAM6QT), the driver tube is 122.5 feet long with an inner diameter of 17.5 inches. It consists of 6 sections of 18-inch schedule-10, type 304 stainless steel pipe, with 1/4 inch thick walls. It is ASME U-stamped and certified for operations up to 300 psig at 200°C [5]. A sting mount is positioned in the diffuser section to allow models to be placed in the tunnel.
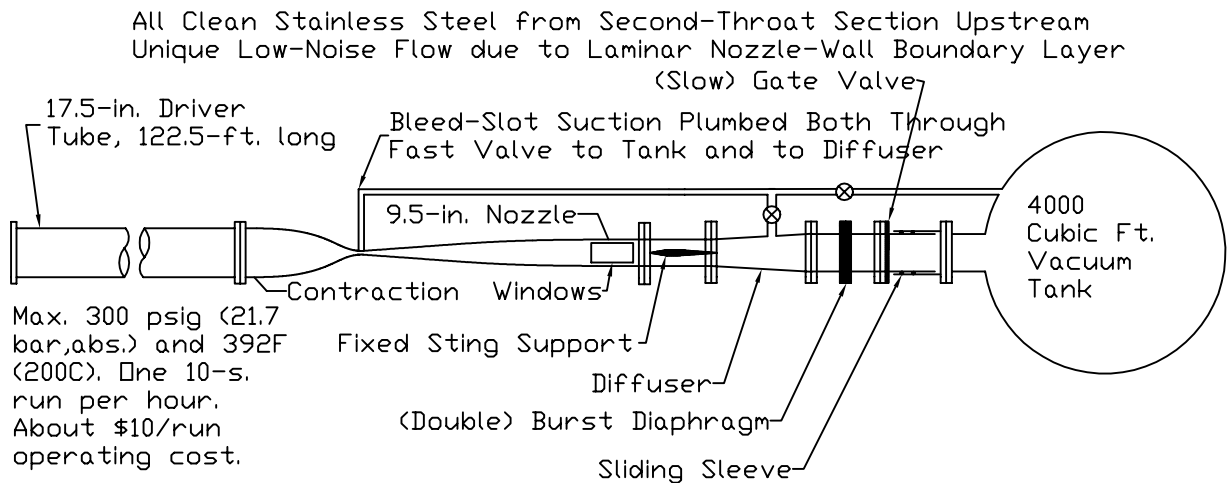
Figure 1.1: The Boeing/AFOSR Mach-6 Quiet Tunnel

Additionally, in order to avoid nitrogen liquefaction in the nozzle at Mach 6, the driver tube must be uniformly heated to about 160°C. To aid in this uniform heating, the driver tube is insulated with 3 inch fiberglass pipe insulation. The tube is heated by generating a 6V electric potential drop across the length of it. This draws approximately 2000 amps through the driver tube, which is heated via Ohm's-law. A thermocouple near the downstream end of the driver tube is typically used to control the temperature, although which thermocouple is the controlling thermocouple can be changed. Four Electronics Measurement Incorporated TCR10T750 power supplies provide the necessary current for heating. These power supplies have a maximum output of 750 amps at 10 volts and are regulated by an Omega CN9000A controller. Starting from room temperature, it takes approximately 6 hours for the driver tube to reach the set temperature and another 18 hours to equilibrate [6].

In order to keep the contraction from being a large heat sink that reduces the temperature of the downstream end of the driver tube, three band heaters are used to heat the contraction. A schematic of the contraction and band heaters can be seen in Figure 1.2. The two upstream heaters are Tempco 1500W, 240V heaters and the smaller downstream heater is a Tempco 3000W, 240V heater. Each heater is controlled by an Athena Controls, Inc., AIM15 controller. Surface thermocouples are affixed to the contraction by hose clamps and are used by the controllers to determine when each heater needs power in order to keep the temperature at the set point.

The three contraction band heaters are typically set to 138, 160, and 160°C, going from the most upstream heater to the most downstream heater. The most upstream heater is always set lower than the other two. It has been found that this enables all three to actually heat the tunnel. Otherwise, the large upstream heater does all the heating. A HEAT 30kW circulation heater, set to 165°C, was used to heat the incoming air. The circulation heater was controlled by a Watlow 988A-10KD-AAGR heater controller. By examining the readout of a thermocouple
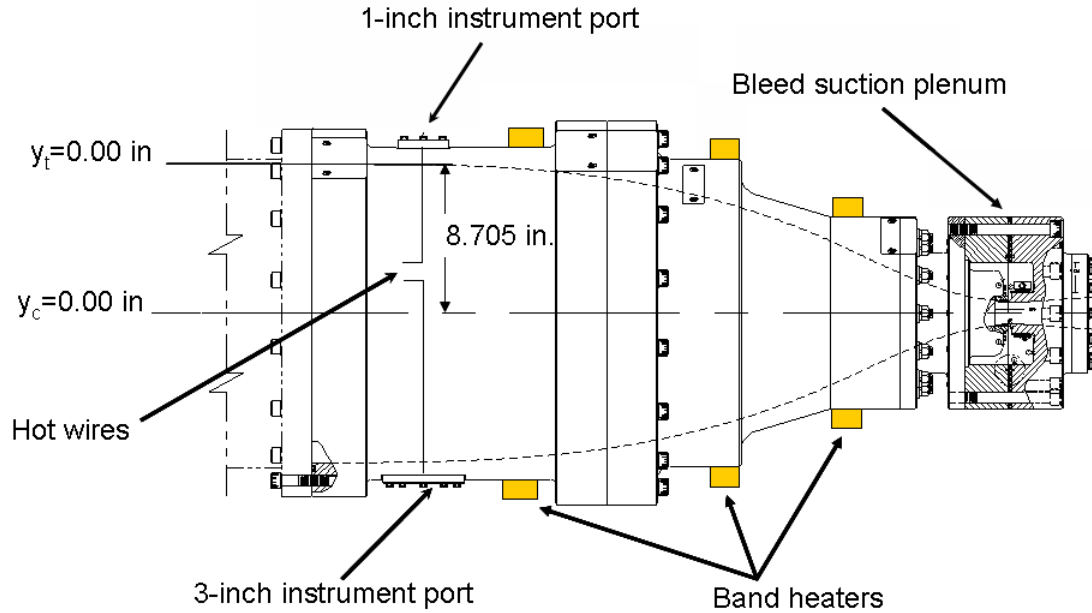
Figure 1.2: Schematic of the contraction

located near the upstream end of the driver tube, it has been found that the actual temperature of the heater equilibrates to about 5°C lower than its set point.

Over the length of the driver tube, a significant boundary layer develops. In Ludwieg tubes, this boundary layer on the driver-tube wall is often turbulent. Although passing through the contraction can relaminarize the boundary layer, it is nevertheless to be removed from the flow just upstream of the throat in order to remove any residual disturbances and to begin with a fresh laminar wall boundary layer with a known starting location [5]. It is to be removed by sucking it through a small axisymmetric bleed slot just upstream of the nozzle throat. The flow through the slot is accelerated to sonic conditions in order to prevent disturbances 1) from feeding upstream and polluting the primary nozzle flow, or 2) causing the location of the bleed-lip stagnation point to oscillate.

The flow through the bleed slot can then be injected back into the main flow downstream of the second throat via the "passive" bleed system or can be exhausted directly into the 4000 cubic foot vacuum tank using the "active" bleed system. The

passive bleed system is activated by the upstream-travelling expansion wave after the diaphragm burst. This allows suction to begin very early into the run. By the time the tunnel has started, the passive bleed-system is started as well. The active bleed-system requires a fast-opening valve to open. The valve is triggered by the oscilloscope and uses the pressure differential across it to open. Thus, depending on the initial stagnation pressure, the active bleed system takes anywhere from 1 to 2 seconds to start. Due to this extended start time, use of the active bleeds significantly reduces the amount of useful data that can be collected during a run, in most cases.

It has been demonstrated that for the passive bleeds with the sting mount positioned in the diffuser, no disturbances due to the reintroduction of bleed flow travel upstream through the subsonic portion of the boundary layer far enough to affect measurements near the nozzle exit. Flow separation caused by shocks from the sting mount prevents any disturbances from travelling that far upstream. With the sting mount removed from the diffuser, however, disturbances due to the reintroduction of bleed flow can be observed far upstream [7].

The nozzle of the BAM6QT was designed and fabricated to very tight tolerances. In an effort to keep wall roughness from being the dominant transition mechanism, it was necessary to ensure that the RMS wall roughness was as small as feasible. Although measurements have not been obtained in the throat, it has been estimated that the RMS in the throat is on the order of 0.5-1.0 microinches. In order to achieve such tight tolerances, it was necessary to make the first 4 sections of the nozzle from one solid piece of electroformed nickel. The remaining 4 sections were machined and polished to obtain an RMS roughness level of approximately 1-2 microinches [8].

The tunnel was always filled in the same manner. The circulation heater was turned on about 30 seconds prior to pressurizing the tunnel. A solenoid on the upstream end of the driver tube was then opened via a remote switch. This allowed air to be pumped into the driver tube. This was accomplished by applying a voltage to a pressure regulator. An incremental increase in this voltage gradually pressurized

the tunnel to the desired initial stagnation pressure. A Panametrics Moisture Target Series-5 dewpoint meter was used to periodically check the dewpoint of the air in the tunnel. This was usually found to be around -20°C, although this value was somewhat higher during the humid summer months.

A pair of burst diaphragms is used to initiate a tunnel run. The gap between the two diaphragms is generally kept at half of the upstream pressure while the tunnel is given time to equilibrate. In order to start a run, the gap is exposed to a vacuum. When the gap pressure drops far enough, the upstream diaphragm bursts, followed soon after by the downstream diaphragm.

At this point, a shock wave travels downstream while an expansion wave travels upstream. The expansion wave traverses the length of the driver tube, in approximately 100 milliseconds, reflecting from the upstream end and then the contraction. Although the nominal tunnel run ends when the expansion wave returns to the contraction, the tunnel has been demonstrated to remain quiet through many expansion-wave reflection cycles. Throughout these cycles, the pressure in the driver tube drops quasi-statically. Given a sufficiently low back pressure, hypersonic flow continues for approximately 6 seconds.

1.2.2   Hurdles in Achieving Quiet Flow

Although the BAM6QT was designed to operate quietly to stagnation pressures of up to 150 psig, the initial tunnel shakedown provided no quiet flow [9] . After testing 6 different bleed slot geometries, a small amount of quiet flow was achieved [10, 11]. Modifying the bleed slot geometry one additional time as well as redesigning the sting supports which secure models in the tunnel yielded consistent quiet flow up to a stagnation pressure of 8 psia [12]. Although a variety of additional tunnel modifications were completed and tested, quiet flow with the electroformed nozzle throat had not been achieved for stagnation pressures higher than 8 psia [13].

Recently, a surrogate aluminum nozzle throat was machined and used in place of the electroformed-nickel throat section. Initially, the surrogate nozzle throat yielded repeatable quiet flow up to almost 20 psia. A 0.002 inch step was then noticed at the downstream end of the surrogate nozzle throat and was reduced, yielding quiet flow to 38 psia. After two cycles of professional polishing and removing damage to the bleed lip, the surrogate nozzle throat was then found to give quiet flow to approximately 95 psia.

Measurements of tunnel noise were made at several axial locations for the original aluminum nozzle as well as after each modification. For all cases, it was found that the flow dropped suddenly into the quiet regime at roughly the same pressure, regardless of axial location. This suggests that there is still some sort of bypass mechanism dominating transition. If linear amplification of instabilities had been the dominating factor in transition, it was expected that the tunnel would be quiet to higher pressures further upstream [7].

Both the original electroformed nozzle throat and the surrogate aluminum nozzle throat were recently precision measured. It was found that the electroformed nozzle throat has a small kink in the contour that is not present in the surrogate nozzle throat nor in the original design. It is thought that this kink is responsible for a separation bubble in the nozzle, limiting quiet flow to only those pressures below 8 psia.

1.2.3   The Need to Examine the Driver-Tube Noise Levels

Until recently, the flow upstream of the throat had not been measured or characterized to determine its role in the early nozzle-wall transition. Noise in the settling chambers of quiet tunnels has been observed to propagate downstream in measurable quantities. It was also thought that sufficiently high noise levels in the flow exiting the driver tube could be a cause of early nozzle-wall transition. These observations and thoughts underscore the importance of examining the flow exiting the driver

tube at the contraction entrance so as to determine if the disturbance levels are within acceptable limits.

Beckwith et al. concluded that the dominant disturbance mode in the settling chambers of blow-down wind tunnels is in the form of acoustic energy. These acoustic disturbances propagate downstream primarily as plane waves [14].

In order to establish whether or not the acoustic disturbances in settling chambers could propagate downstream and be observed in the supersonic test sections of blow-down tunnels, a theoretical model of acoustic plane wave propagation was developed and compared to empirical results from several facilities. It was assumed that these acoustic disturbances travel as plane waves in an irrotational isentropic flow. Thus, for sufficiently high free stream Mach number flows, the conservation of acoustic energy flux was used [15].

Of the acoustic disturbances present in settling chambers, it is estimated that somewhere between 20% and 40% of this energy is transmitted into the test section of supersonic tunnels. It was found that empirical results agree well with theory for Mach numbers up to at least 5 and frequencies up to 60 kHz [14, 15]. However, these facilities had much smaller contraction ratios than the BAM6QT, around 88. The contraction of the BAM6QT most likely reflects much more of the noise back into the driver tube since its contraction-area ratio is about 145.

Experiments were carried out to ascertain the effects of transmitted settling chamber noise on test section noise levels and flow characteristics. In supersonic wind-tunnel tests at JPL, it was found that for a free stream Mach number of 1.78, settling chamber turbulence levels had a strong affect on transition Reynolds numbers for models in the test section. No such effect was observed for Mach numbers between 2.55 and 4.5 [16]. This behavior was also observed in independent tests at Mach 5 in a NASA Langley tunnel. A settling chamber noise increase from 0.35% to 0.85% caused no measurable increase in free stream noise levels [17].

Contrary to these findings, it was observed, in an initial examination, that transition on sharp cones in the Langley Mach-8 Variable Density Tunnel was significantly

affected by upstream disturbances. Various configurations of upstream valving and screens provided changes in settling chamber noise levels. Furthermore, additional Mach 5 data indicate that RMS pitot-pressure levels and trends had some dependency on settling chamber screen configuration [18].

Beckwith et al. completed detailed studies of methods for attenuating the observed noise in the settling chambers of supersonic wind tunnels. In a pilot quiet facility at NASA Langley with Mach 5 nozzles, noise levels in the settling chamber were reduced from an unspecified amount to below 1% with the use of "acoustic baffles" and screens. The acoustic baffles consisted of porous Rigimesh plates. About 12 inches of steel wool were then added to the settling chamber. This further reduced the fluctuation levels to about 0.2% [14]. NASA Langley also used such acoustic baffles in the settling chamber of the Supersonic Pilot Tunnel. Though this facility had mass flows nearly an order of magnitude higher than that of the Mach 5 facility, settling chamber noise was again very effectively reduced [15].

Clearly, it is uncertain what settling chamber noise levels are acceptable. Considering the success NASA Langley has had in the area of operational quiet tunnels, it is inferred that if the driver tube of the BAM6QT has noise levels comparable to those present in the quiet Langley tunnels, they are within an acceptable range. Beckwith suggested that total disturbance levels in the settling chambers of quiet tunnels should be reduced to 1% or less [17]. If this is not found to be the case, there are a number of relatively easy and inexpensive components that could be added to attenuate noise levels appreciably. However, these solutions may not work in a Ludwieg tube due to the short run time.

1.3   Hot Wires

One common fluid-mechanics measurement tool is the hot wire. A hot-wire probe consists of a length of very fine wire (on the order of 0.0001 inches in diameter) welded between two probe arms. The probe is then typically connected to a constant tem-

perature anemometer (CTA), a constant current anemometer (CCA), or a constant voltage anemometer (CVA). The CTA and CCA are the most common anemometers used and will be the only two discussed [19].

A hot wire acts as the fourth leg of a Wheatstone bridge electronic circuit. A CTA schematic can be seen in Figure 1.3. The CTA operates by holding the hot wire at a fixed temperature that is higher than the surrounding fluid. As the fluid flows past the wire, the amount of heat transfer from the wire into the fluid changes with changes in the flow.
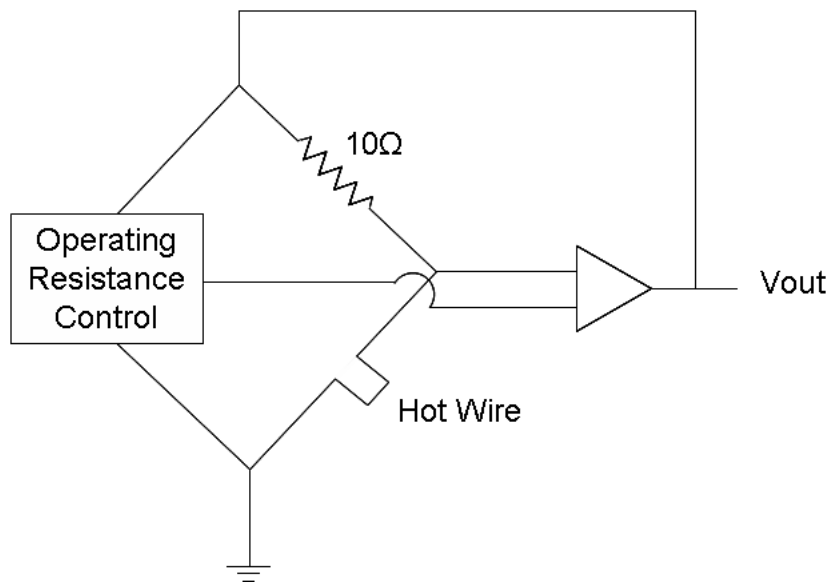
Figure 1.3: Simplified CTA circuit

This changing heat flux serves to change the wire temperature. This unbalances the Wheatstone bridge. The amplifier responds very rapidly by changing the voltage drop across the wire. This serves to change the wire temperature, and thus its resistance, back to the original set value, effectively balancing the bridge. By recording this 'bridge' voltage, it is possible to infer the mass flow of the fluid past the wire.

When operated in CCA mode, the anemometer circuit looks much the same. Here, however, the fixed resisters are much higher (three orders of magnitude) than in the CTA. This allows very little current to flow through the hot wire, and thus wire

heating is negligible. The wire temperature is then essentially equal to the free stream recovery temperature. A schematic of a CCA circuit can be seen in Figure 1.4. The recorded bridge voltage allows the resistance of the wire to be calculated. The wire temperature can then be found from a simple resistance-temperature wire calibration in an oven. The flow temperature can then be inferred from the known recovery factor. In a low-speed flow, such as that in the contraction, the recovery factor is taken to be one [20]. This allows accurate temperature measurements to be easily obtained.
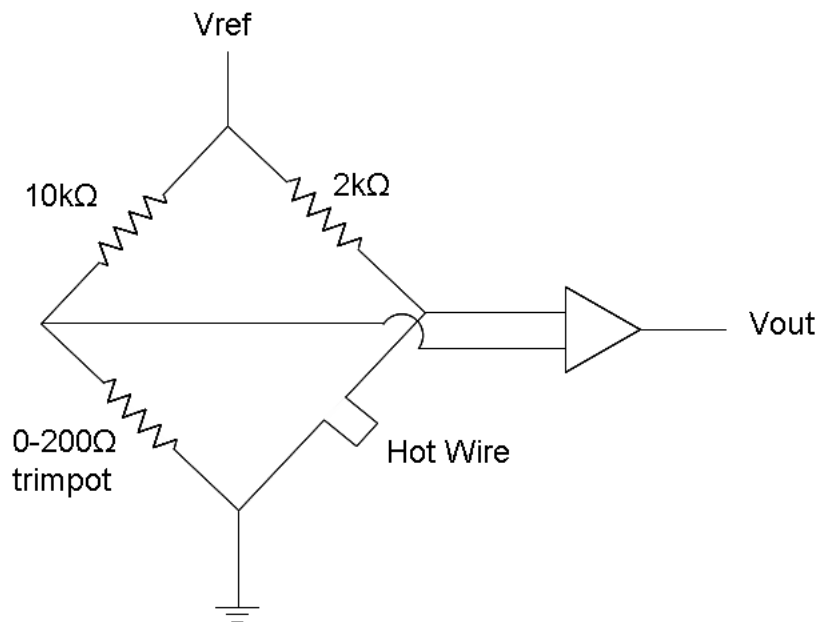
Figure 1.4: Simplified CCA circuit

2. Apparatus

It is not easy to make measurements in the driver-tube exit or contraction entrance, since both the driver tube and contraction are ASME code-stamped pressure vessels, and not readily modified. However, measurements are possible using two access ports provided at the entrance to the contraction, near the driver tube exit. The access ports are centered 6.500 inches downstream of the beginning of the contraction, where the tunnel radius has only decreased from 8.750 inches in the driver tube to 8.705 inches [21]. The bottom access port has a diameter of 3.000 inches while the top access port has a diameter of 1.000 inch. The locations of the access ports can be seen in Figure 1.2.

In order to utilize the 1-inch diameter port in the top of the contraction, a traverse mount was designed and used in the tunnel. The mount, made of 0.25-inch aluminum, can be seen in Figure 2.1. It was attached to the 1-inch blank via four 1/4-20 bolts screwed into the push-off holes in the blank. Clearance holes in the base allowed access to the three 1/4-20 bolts, allowing the blank, traverse, traverse mount, and probe to be removed from the tunnel simultaneously. The hot-wire position in the contraction was changed by adjusting the lead screw of the traverse holding the probe support.

A Velmex A2509BE-S2.5 Unislide traverse allowing 6.5 inches of vertical movement and a Velmex A2515BE-S2.5 Unislide traverse allowing 13.0 inches of vertical movement were used to position the hot-wire probes in the contraction. Both traverses are equipped with a Vernier scale allowing positioning to within 0.001 inches.

Both probes were positioned in the probe supports by removing the blanks from the contraction and inserting the appropriate hardware. Thus the distance between the probe and the contraction wall could be measured using digital calipers. A visual inspection estimates the error in initial probe position to be 0.01 inches. Thus, the

Figure 2.1: Traverse and mount used for contraction measurements

precise distance the probe was moved could be readily determined, but the actual position error was set by the initial uncertainty. Two 18-inch TSI 1160-18 high-temperature probe-supports were used to support the probes in the tunnel.

TSI 1222-P12.5 high temperature hot-wire probes were used for both hot-wire and cold-wire investigations. Platinum/10% Rhodium (Pt/Rh) wires were used for all contraction measurements. They had a diameter of 0.00015 inches and a length/diameter ratio of approximately 340. A picture of one of the probes positioned in the tunnel can be seen in Figure 2.2. The apparent bend in the probe support at the top of the picture is simply an artifact of the camera lens. The probes were inserted into the contraction via the access ports as seen in Figure 1.2. A close-up picture of the probe and the wire can be seen in Figure 2.3. For scale, the probe needles in Figure 2.3b are separated by 0.055 inches.
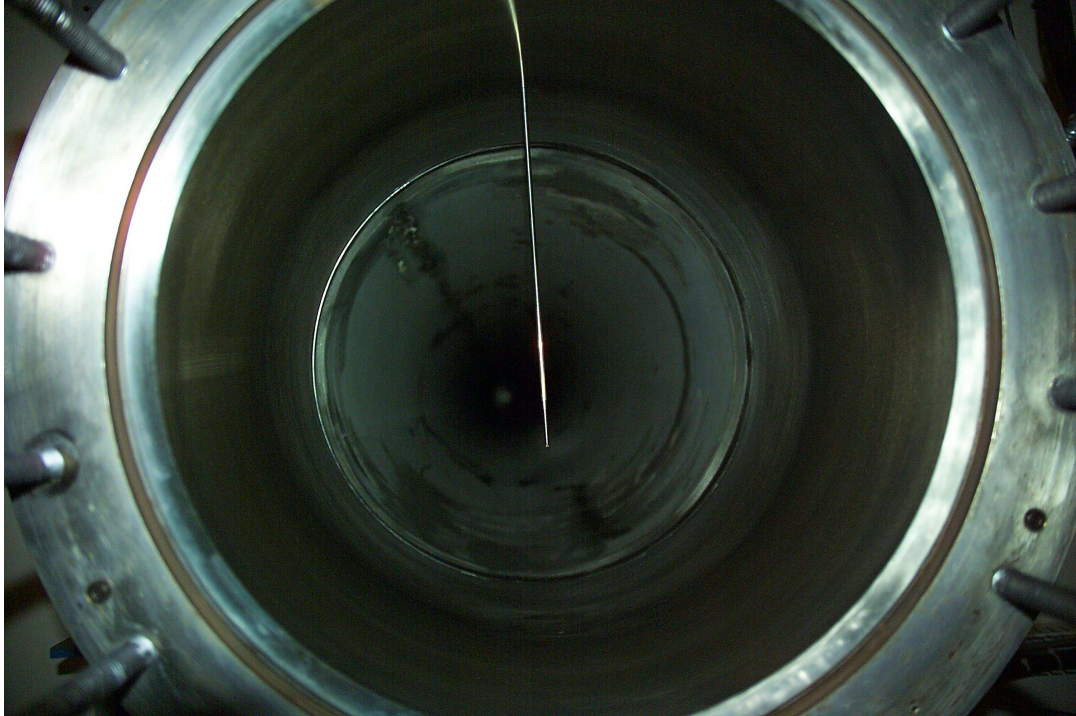
Figure 2.2: Hot-wire probe positioned in the contraction entrance looking upstream into the driver tube
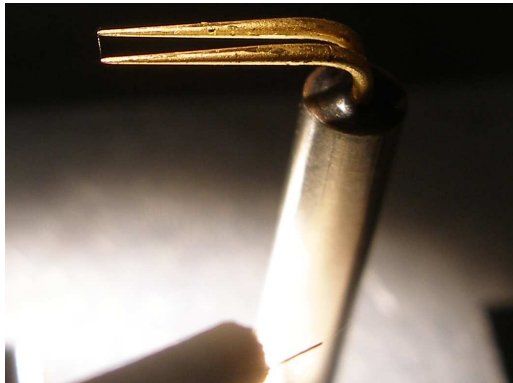
(a) Typical hot-wire probe

(b) Close up of hot-wire probe tip and wire

Figure 2.3: Typical hot-wire probe

When the probe was operated in constant current mode, an in-house constant current anemometer (CCA) was used to power the probe and condition the probe's output signal. Two outputs are available from the anemometer, a DC signal with a

gain of 100, and a high-pass filtered AC signal with a gain of 10,000. The high-pass filter is a simple RC filter with a design point of 800 Hz.

For hot-wire applications, a TSI IFA-100 constant temperature anemometer (CTA) was utilized. The CTA was operated using the standard-2 bridge.

Kulite pressure transducers were used to record pressures in a number of tunnel locations. A Kulite model XTEL-190-200A was wall-mounted in the 3-inch port at the entrance to the contraction. A Kulite XT-123CE-190-300SG transducer was used for pressure measurements in the bleed suction plenum. Both of these locations can be seen in Figure 1.2.

Kulite XCQ-062-15A transducers were used to measure pitot pressure on the tunnel centerline at an axial location of z=75.3 inches (where the nozzle throat is at z=0.0 inches). These transducers were modified by the manufacturer so that the transducer diaphragm was physically stopped above about 15 psia. This allowed high pressure-resolution data to be recorded during a tunnel run, when the pitot pressure is typically less than 2 psia, while protecting the sensor from damage during the substantially higher pre-run pressures. The stock pressure transducers are designed to maintain their calibration for pressures up to twice the design pressure, 15 psia in this case, and to survive only up to three times the design pressure, well below the maximum pressure seen in the tunnel. Additionally, a temperature-sensing wire was added to the output to allow calibration adjustments for variations in the transducer temperature.

All pressure transducers were used in conjunction with in-house electronics used to power the sensors and condition the output signal. One output was the DC signal with a gain of 100. The other was high-pass filtered at 800Hz with a gain of 10,000, effectively isolating the AC component of the signal.

Data were recorded on one of four oscilloscopes. A Tektronix TDS7104 digital oscilloscope operating in Hi-Res mode was used to capture all hot and cold-wire data. In Hi-Res mode, the oscilloscope samples data at a rate of 1 GS/sec and then averages it into memory at the set sampling frequency. A Tektronix TDS5034B digital

oscilloscope operating in Hi-Res mode was used to capture some static-pressure data in the contraction. For timescales of 1 second/division, the Tektronix oscilloscopes in Hi-Res mode gives 15 bit resolution. A LeCroy 9314AL and a LeCroy 9304AM digital oscilloscope were used to record additional data. The 9314AL sampled data at 100kS/second while the 9304AM sampled at 25kS/second. Both gave 8 bit resolution. Only the bleed-slot plenum data were ever recorded on this oscilloscope.

A Paroscientific, Inc. Model 740 digital pressure gauge (0-400 psia) was used to monitor the pre-run pressure upstream of the burst diaphragms. It was also used to obtain pressure data for the pressure-transducer calibrations. This quartz-beam gauge is very stable and accurate to 0.01% of full scale.

3. Free Convection

3.1 Free Convection in the Air

One of the possibilities for generating noise in the contraction entrance is free convection in the nominally stagnant driver-tube air, prior to the beginning of the run. If free convection exists and sets up significant nonuniformities in the air, they could convect downstream once flow has begun, and cause increased noise or even early transition.

Initial hot-wire measurements were made with atypical tunnel temperature settings. The driver tube temperature, normally 160°C, was heated to only 100°C while the contraction band heaters were turned off altogether to allow the contraction to be opened. The circulation heater was set to 105°C. Since the temperature was already turned down, several tunnel runs were made to collect data at this atypical tunnel setup. The hot wire had an overheat ratio, defined as the ratio of the heated-wire resistance to the unheated wire resistance with the wire in the contraction, of 1.64.

In the course of examining the run data, large fluctuations were noticed in both the pre-run and the run data. It was hypothesized that free convection due to the non-uniform contraction/driver-tube heating could have been the cause. In order to investigate this theory, several oscilloscope traces were recorded for stagnant air. These could then be compared to similar traces with a fully heated contraction. The hot wire was positioned 7.77 inches above the contraction centerline, 0.94 inches below the top contraction wall. The stagnant-air traces were recorded for a pressure of approximately 25 psia, about 25 minutes after the driver tube was pressurized.

The driver tube was then fully heated to 160°C and the contraction heaters were returned to their nominal set points. This should have given a uniform driver tube and contraction temperature of approximately 160°C. During the heating process,

the hot wire broke. A different probe of the same type was then used to collect the heated tunnel data.

With the tunnel heated and the wire tuned to obtain the maximum frequency response, the best hot-wire overheat ratio that could be obtained was only 1.09. In this state, the hot wire was on the verge of being unstable and thus was very susceptible to electrical oscillations. The operating resistance could not be adjusted any higher without causing the hot-wire output to oscillate. These oscillations disrupt the normal wire output and also often cause the wire to break. It is thought that the low overheat ratio obtained was because the effective "cold" temperature of the wire was already 160°C due to tunnel heating. In order to obtain a better overheat ratio, the hot wire was slightly "detuned" and was no longer set for maximum frequency response. This meant that the hot wire was much more stable, and an overheat ratio of 1.52 was achieved. This typically kept the hot wire fixed at about 500°C.

The tunnel was pressurized to approximately 25 psia and the hot wire was positioned 0.94 inches below the top contraction wall, as before. Oscilloscope traces were recorded over 10 minute intervals for 90 minutes. Figure 3.1 shows the oscilloscope record for the cooled contraction after about 25 minutes (3.1a), and the heated contraction after 30 minutes (3.1b).

(a) Unheated contraction after about 25 min.   (b) Hot contraction after 30 min.
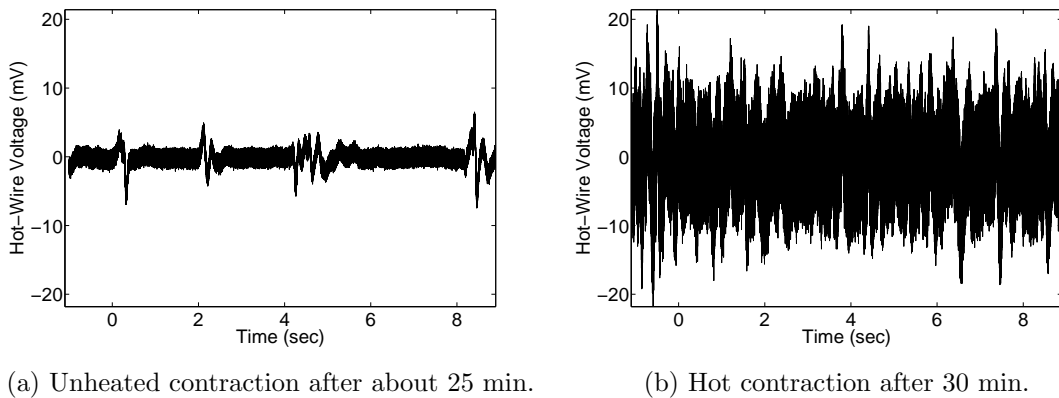
Figure 3.1: Hot-wire traces for fully heated and partially heated contractions at 25 psia and y_t=0.94 in.

As can be seen, the fluctuations are about three times larger in magnitude and much more frequent for the case of the fully heated driver tube and contraction. Despite the somewhat lower overheat ratio and the new probe, this result was surprising. When the contraction was cooled, the driver tube was still heated to approximately 100°C. This resulted in a large temperature gradient over the length of the contraction. It was thought that this large temperature gradient could have been responsible for inducing free convection in the contraction section, and thus the intermittent fluctuations observed in Figure 3.1a.

Another possible explanation is that the observed free convection is caused by an axial temperature gradient across the nozzle throat. A large temperature gradient occurs here because there are no tunnel locations downstream of the throat that are heated. Thus, the stagnant air downstream of the throat is much cooler than that upstream. It is possible that some of this cooler air feeds back upstream through the throat and into the contraction. This would introduce free convective currents in the contraction.

It was thought that keeping the tunnel and contraction section heated to approximately 160°C would remove the tunnel temperature nonuniformity, and thus remove or lessen free convection due to differences in wall temperature and air temperature within the contraction. This would be evidenced by smaller fluctuations in the CTA output signal. However, this was not the case. Instead, the fluctuations with a nominally uniform tunnel temperature were about a factor of three larger than those recorded for the cooled contraction. This might be attributed to the fact that the downstream section of the contraction near the 1-inch nozzle throat was not heated. Since the driver tube was heated to 160°C, not 100°C as in Figure 3.1b, an even larger temperature gradient existed near the end of the contraction for the fully heated case, leading to larger free-convection disturbances either from the wall-temperature differences or again from cooler air feeding upstream through the nozzle throat. Further experimentation was done to ascertain the effect of location and time on free convection effects.

For this study, an overheat ratio of 1.62 was used for all data recorded. The driver tube and contraction temperatures were set to 160°C. All oscilloscope traces were recorded with a sampling frequency of 500 kS/s.

The tunnel was pressurized to approximately 26 psia. Ten-second oscilloscope traces were recorded every 10 minutes over a period of 2 hours at y_t=0.10, 0.35, 0.60, 1.10, 1.35 inches at a sampling rate of 250kS/sec. Traces were also recorded every 10 minutes over an 80 minute period at a wall distance of 0.85 inches. Additionally, traces were recorded over a 30 minute period for hot-wire locations of 1.50 inches to 6.50 inches below the top tunnel wall, in 0.50 inch increments.

These later records were taken over a shorter time period because no obvious temporal dependency was observed in the oscilloscope traces. Figure 3.2 shows the hot-wire RMS voltage, found over time periods of 0.02 seconds, plotted against time after the driver tube was pressurized to 26 psia, at $y_t = 0.60$ inches. As can be seen, there is no apparent temporal dependency. Here, the electronic noise was subtracted from the hot-wire signal by finding the square root of the difference between the square of the hot-wire signal RMS and the square of the electronic RMS noise. The electronic noise was found by recording a voltage trace at low pressure and finding the RMS. Figure 3.3 shows two sample oscilloscope traces taken 30 and 120 minutes after the driver tube was pressurized at $y_t = -0.60$ inches. No major qualitative difference can be observed.

Figures 3.4a, 3.4b, and 3.4c are typical oscilloscope traces for y_t= 0.10, 3.00, and 6.50 inches, respectively, for a driver-tube pressure of 26 psia. As can be seen in these figures, the RMS level does seem to have a dependency on wall distance.

Figure 3.5 underscores this observation by showing the RMS plotted against y_t for times of 0, 10, 20, and 30 minutes after the driver tube was pressurized to 26 psia. The average RMS was found by breaking each trace up into segments of length 0.02 seconds, finding the RMS of each segment, and then averaging the RMS value of all the segments. Here, the electronic noise was not subtracted. For some voltage traces, the measured noise levels were indistinguishable from the calculated electronic
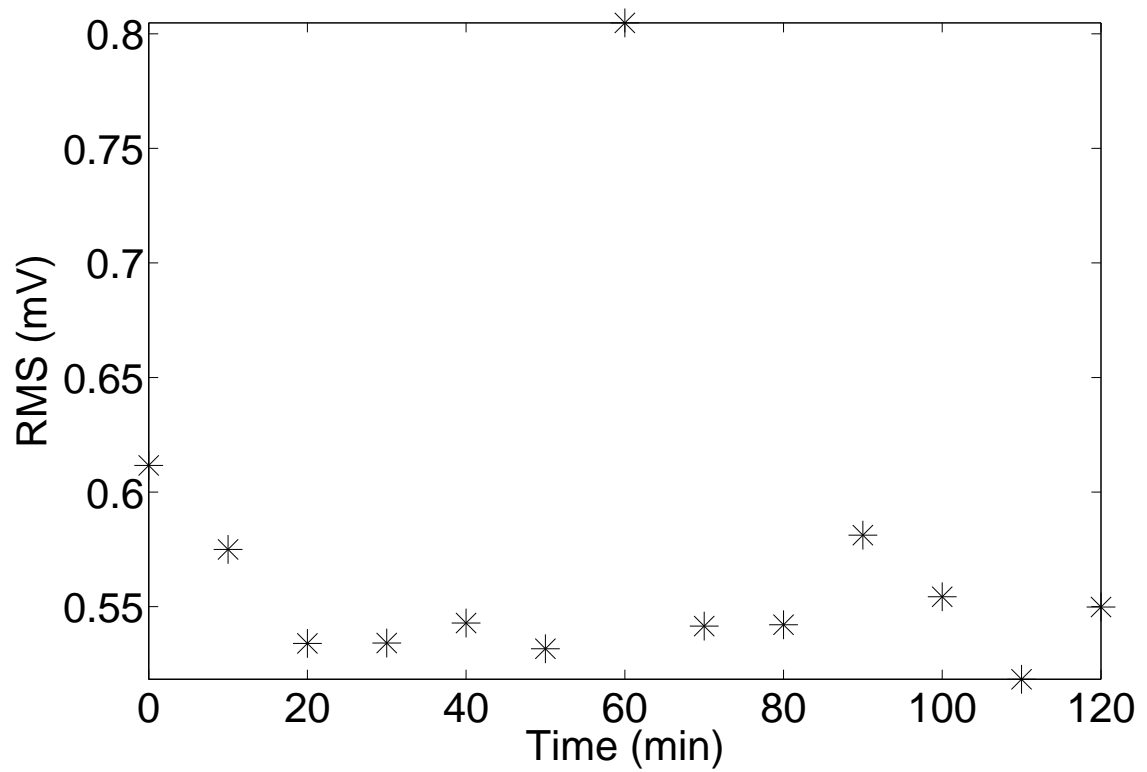
Figure 3.2: Hot-wire RMS voltage vs. time for y_t=0.60 inches.
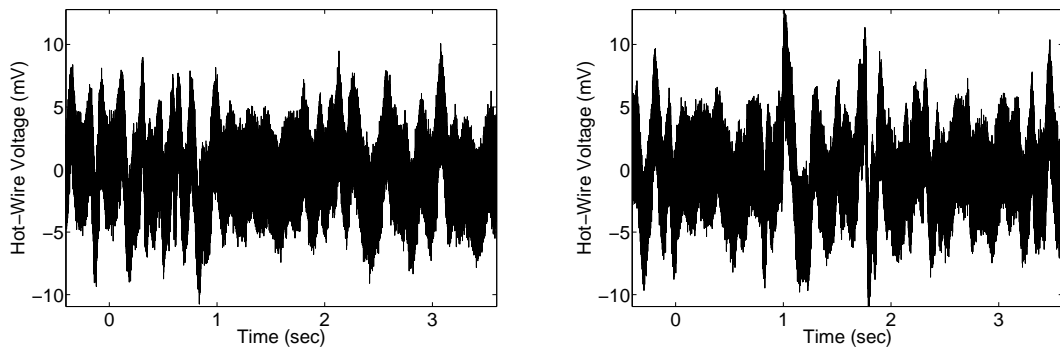
(a) Sample oscilloscope trace at $y_t = 0.60$ in after 30 minutes

(b) Sample oscilloscope trace at $y_t = 0.60$ in after 120 minutes

Figure 3.3: Hot-wire traces after settling times of 30 and 120 minutes
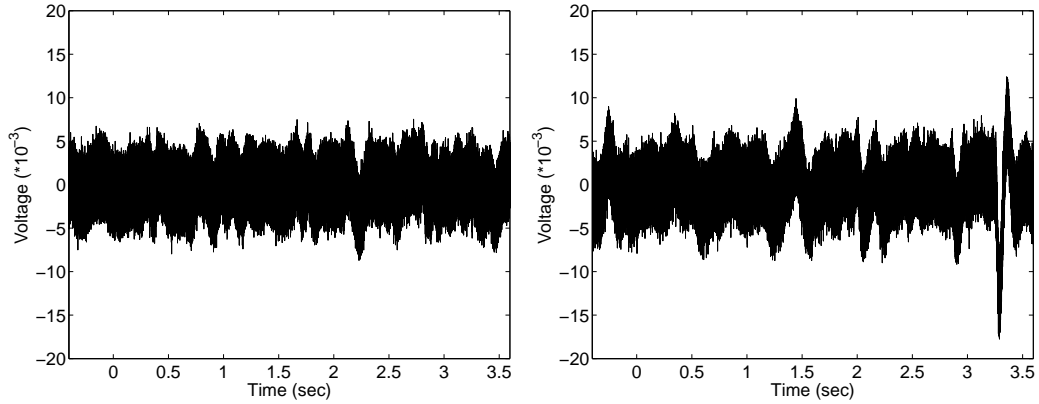
(a) Sample oscilloscope trace at $y_t = 0.10$ in after 30 minutes

(b) Sample oscilloscope trace at $y_t = 3.00$ in after 30 minutes
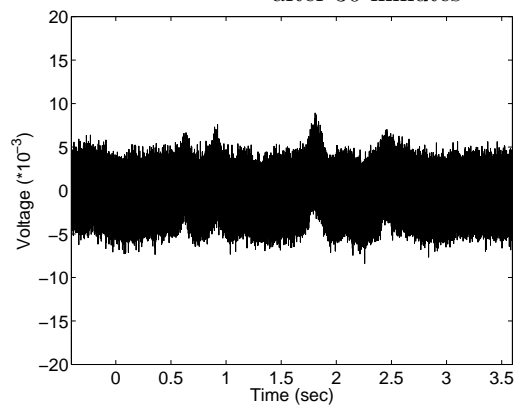
(c) Sample oscilloscope trace at $y_t = 6.00$ in after 30 minutes

Figure 3.4: Hot-wire traces for various wall distances and RMS

noise, and at times was found to be slightly less than the electronic noise. Due to the manner in which the electronic noise was subtracted, this lead to some imaginary RMS values.

Again, the lack of any temporal dependence can be seen. Additionally, the average RMS 0.10 inches from the wall is near the RMS levels observed from 3.00 to 6.50 inches from the wall. The average RMS then drops sharply and then increases rapidly to a maximum value around 1.50 inches from the contraction wall. The RMS then recovers to a nearly constant lower value between 3.00 and 6.50 inches from the wall.
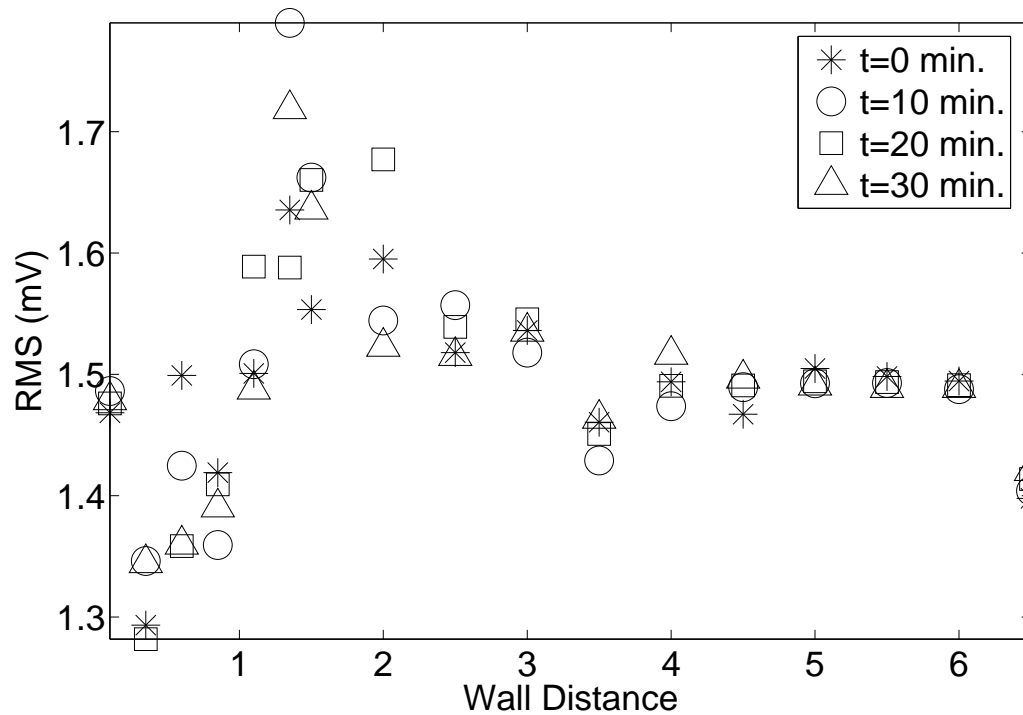
Figure 3.5: Average RMS vs. wall distance

This behavior was unexpected. It was thought that if a wall effect were causing the observed free convection, the effects would be greatest near the wall and then decrease as distance from the wall increased. This is clearly not the case.

It was thought that an examination of the temperature profile in the contraction would provide an explanation for this unexpected behavior. A detailed discussion of the contraction temperature is presented in Chapter 4.

3.2   Free Convection From the Wire

Free convection due to the difference in wire temperature and air temperature could also introduce disturbances into the flow. Fingerson and Freymuth [22] state

that free convection effects from hot wires can be neglected in flows where the Grashof number raised to the 1/3 power is less than the wire Reynolds number.

The Grashof number is a nondimensional number that describes the ratio of the buoyancy force of the fluid to the inertial force. The Grashof number is given by:

$$Gr = \frac{g\beta(T_w - T_0)d^3}{\nu^2} \tag{3.1}$$

where Gr is the Grashof number, g is acceleration due to gravity, β is the coefficient of expansion for air, T_w is the wire temperature, T_0 is the flow temperature, d is the wire diameter, and ν is the dynamic viscosity.

Figure 3.6 shows the Grashof number raised to the 1/3 vs. wire Reynolds number for the full range of wire Reynolds numbers present in the contraction. As can be seen, $Gr^{\frac{1}{3}} << Re_w$ in all cases. Thus, while the tunnel is running, free convection from the wire into the flow can be neglected as a source of disturbances. It is possible that when there is no flow in the tunnel, free convection from the heated wire could affect measurements. However, a method of determining this effect is not known.
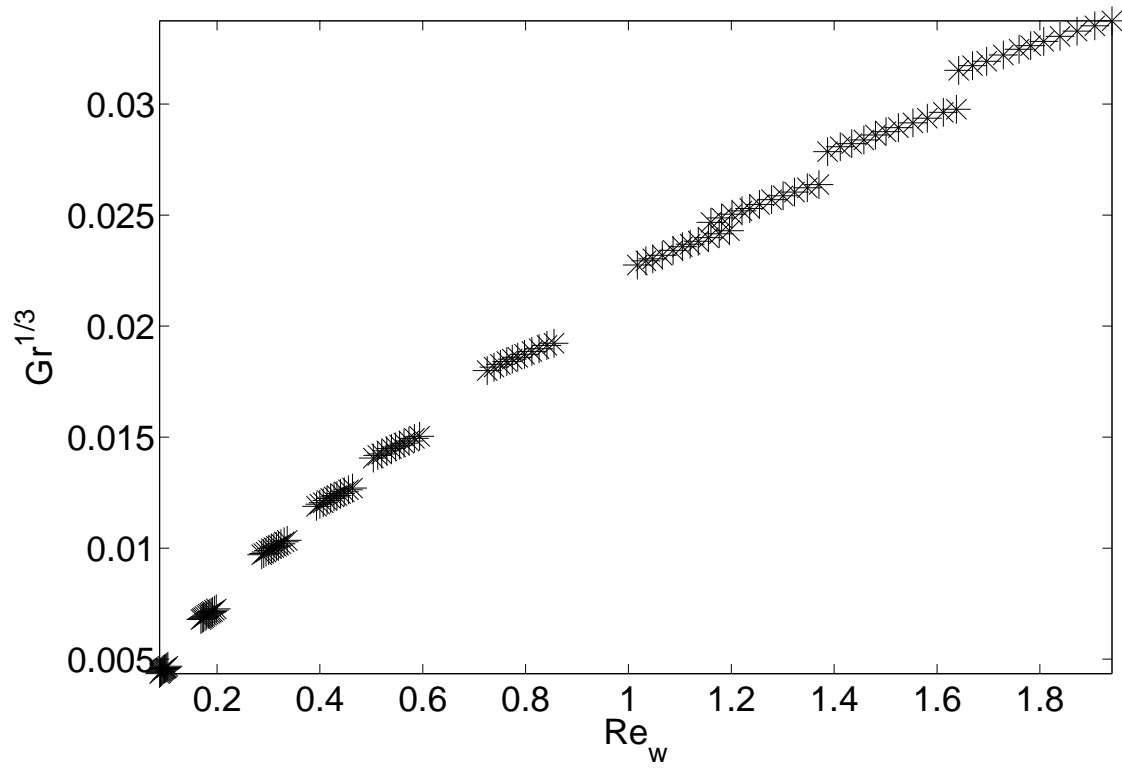
Figure 3.6: $Gr^{\frac{1}{3}}$ vs. Re_w for all contraction Reynolds numbers

4. Temperature Profile and Fluctuations

4.1 Introduction

In order to help explain the observed pre-run free convection in the contraction, temperature profiles were measured in the contraction for several different initial stagnation pressures. It is possible that a sufficiently large temperature gradient could have been responsible for the free convection. If such a gradient also existed in the driver tube, it could have a negative impact on flow quality, introducing undesired disturbances and creating a generally non-uniform flow. These non-uniformities and disturbances could be washed downstream and augment noise levels in the contraction and/or adversely affect the nozzle-wall boundary layer transition.

The air temperature was easily calculated using a set of simple calibrations. The resistance of the hot wire should vary linearly with temperature. Likewise, the CCA output voltage should be a linear function of the resistance supplied by the wire.

To calibrate the CCA, a number of different resistors were substituted into the Wheatstone bridge circuit in place of a hot wire. The resistance as well as the CCA output voltage were measured using an HP 34401A digital multimeter and recorded.

The calibration of a hot wire was a somewhat more involved task. The wire, inserted in one of the high-temperature probe supports, was positioned in either a Blueline 0V480 or a School-Tech, Inc. 14303W2 electric oven. The oven temperature was set and it was allowed to equilibrate. The oven air temperature was measured using a K-type thermocouple and a Fluke 51II digital thermometer. The thermocouple tip was positioned approximately 1 inch below the hot wire. After sufficient time had passed (the heating light had gone off and had to come back on again), the wire resistance and air temperature were recorded.

Figure 4.1a shows one such CCA calibration. Figure 4.1b shows a sample wire-temperature calibration. For all wires used throughout the course of experimentation, the temperature/resistance relationship was observed to be very linear.

(a) CCA output voltage vs. resistance

(b) Temperature/resistance calibration for a hot wire
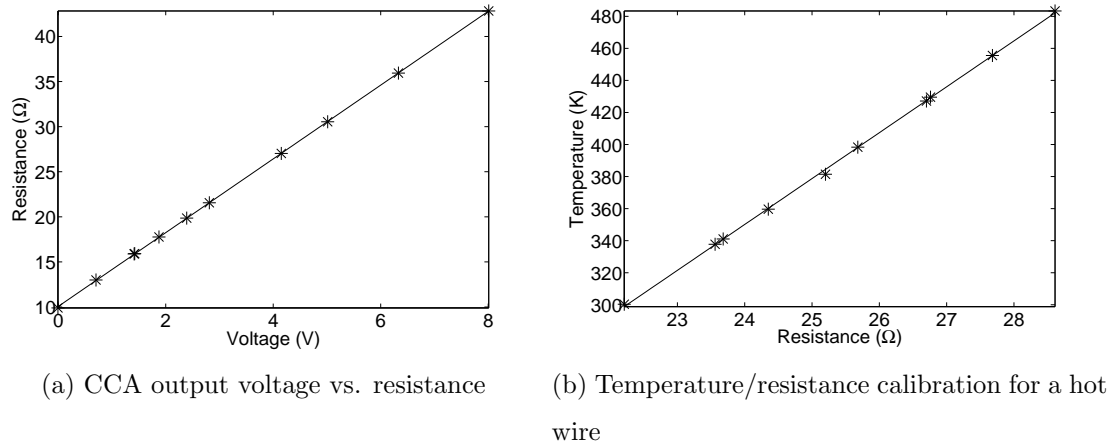
Figure 4.1: CCA and hot-wire calibrations

4.2   Preliminary Measurements

In order to obtain temperature information in the contraction, the hot wire was operated in constant-current mode. All runs were sampled at 200KS/sec for 10 seconds in Hi-Res mode. As before, the recovery factor was taken to be 1.

Due to traverse limitations, the lowest point the wire could reach in the contraction was 3.00 inches below the centerline (although the diameter was 17.41 inches). Measurements were made for locations of y_c=-3.00, -2.00, -1.00, 0.00, 1.00, 2.00, 3.00, 6.00, and 8.00 inches with the tunnel centerline being y_c=0.00 inches. Measurements were made for initial driver-tube pressures of 8, 90, and 145 psia. Locations from y_c=-3.00 to 2.00 inches were measured first for each pressure. The probe support was then moved up on the traverse to allow the wire to reach locations of y_c=3.00, 6.00, and 8.00 inches. For these runs, the driver tube temperature was set to 160°C. The tunnel was filled in the usual manner.

Figures 4.2a-4.2c show temperature as a function of distance from the centerline in the contraction, for times of -0.5 seconds to 5.5 seconds in 1 second intervals with 0 seconds being the time the run was initiated. Thus, the points corresponding to -0.5 seconds correspond to the pre-run temperature. Each point shows the temperature averaged over 0.25 seconds. Figures 4.2d-4.2f show the temperature as a function of time for the aforementioned contraction locations.

As expected, the temperature trend for all values of y_c examined was that temperature dropped with time. This was due to the isentropic expansion of the driver-tube gas from the passing expansion waves.

Unexpectedly, the pre-run temperature at the two locations closest to the upper wall, y_c=6.0 and 8.0 inches (0.705 and 2.705 inches from the top tunnel wall, respectively) were much higher than the set point of 160°C. With a uniformly heated and insulated driver tube, and a uniformly heated contraction, it was expected that the air temperature for all y_c would be very close to 160°C. As can be seen in the figures, the temperature at these locations is the highest for all pre-run data points and decreases slightly with increased initial driver-tube pressure. For locations closer to the tunnel centerline, the pre-run temperature was much closer to the expected value.

For the y_c=6.00 and 8.00 inch cases, the temperature drops off very rapidly after the beginning of the run and approaches a temperature near what was measured at other locations, though the temperature remains consistently higher than those measured at other locations. Due to the rapid temperature drop-off at these locations, it is thought that the high pre-run temperatures are due to overheating of the contraction, not the driver tube. Since measurements were made at the contraction entrance, the pre-run temperature is the only one that reflects the temperature of the air heated in the contraction. Points for temperatures during a run are primarily the temperatures of air heated in the driver tube. After the flow begins, the air in the contraction entrance moves at about 5.5 feet/second. By the time the second data point at 0.5 seconds is calculated, most of the air present in the contraction
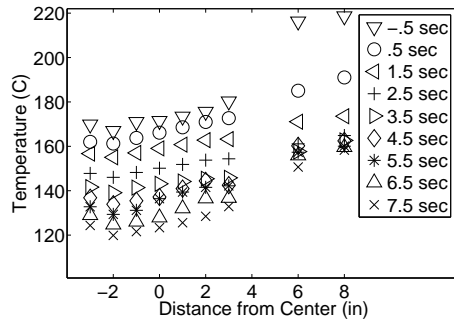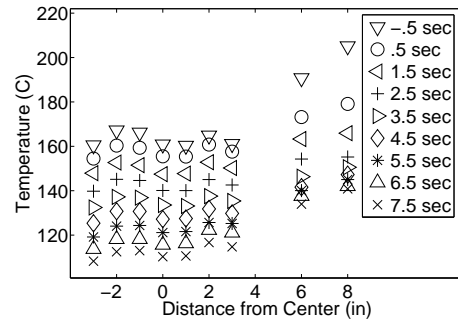
(a) Driver tube initial pressure of 8 psia

(b) Driver tube initial pressure of 90 psia
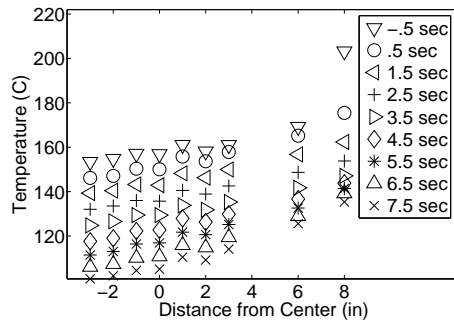
(c) Driver tube initial pressure of 145 psia
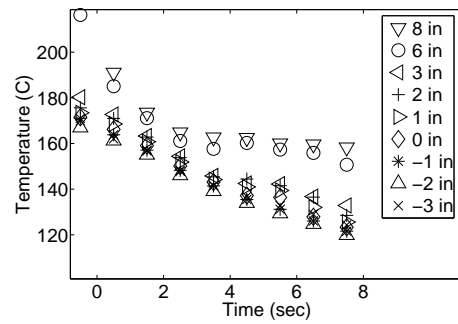
(d) Driver tube initial pressure of 8 psia
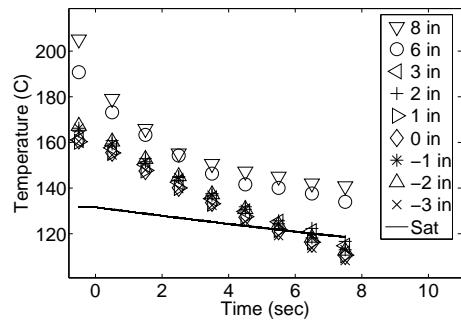
(e) Driver tube initial pressure of 90 psia
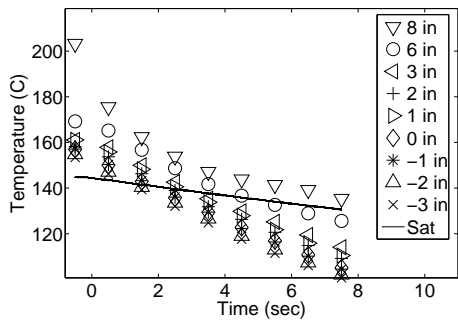
(f) Driver tube initial pressure of 145 psia

Figure 4.2: Temperature profile of full-temperature driver tube for 8, 90, and 145 psia

prior to a run has been evacuated into the nozzle and bleed system and replaced by air from the driver tube.

It was surprising that the 8 psia runs yielded pre-run temperatures nearly 20°C higher than the pre-run temperatures at the same location for 90 and 145 psia. For the 8 psia runs, there was typically around 45 minutes of equilibration time after the tunnel had been set to the desired pressure. The long wait time was because the vacuum pump took a good deal of time to pump the vacuum tank to below 1 torr. This low back pressure was needed in order to extend the duration of supersonic flow. Runs at an initial driver-tube pressure of 90 psia equilibrated for approximately 15-20 minutes, although several runs equilibrated for over 30 minutes. Runs at 145 psia equilibrated for around 10-15 minutes, although several runs equilibrated for over 30 minutes as well. Since the 8 psia runs were exposed to the hot inner contraction wall temperature somewhat longer than the other pressure cases, it makes sense that all temperatures were significantly higher than those at the other two pressures. Thus, for the uneven contraction heating, a longer equilibration time does not necessarily provide more uniform temperatures in the driver tube and contraction.

It was thought that the higher pre-run temperatures near the wall were due to the manner in which the contraction heating was controlled. There are 3 band heaters on the contraction. A J-type thermocouple is attached to the contraction very near each band heater using simple hose clamps. An photograph of one of the thermocouples is shown in Figure 4.3. The temperature sensed by the thermocouple is used by the band-heater power supply to determine when each heater is in need of power. It is thought that since the outer wall of the contraction that is not directly underneath the band heaters is exposed to room-temperature air, the outer surface of the contraction is cooled significantly with respect to the inner contraction wall. Thus, while the outer contraction wall slightly away from the band heaters is maintained at 160°C, the inner contraction wall has a much higher temperature.

It is also possible that the thermocouples read a misleadingly lower temperature since they were also exposed to room temperature air. This would allow more heat from the thermocouples to be transferred into the room air, giving an artificially

low temperature reading. The power supply would interpret this as a call for more power to the band heaters, raising the contraction temperature.
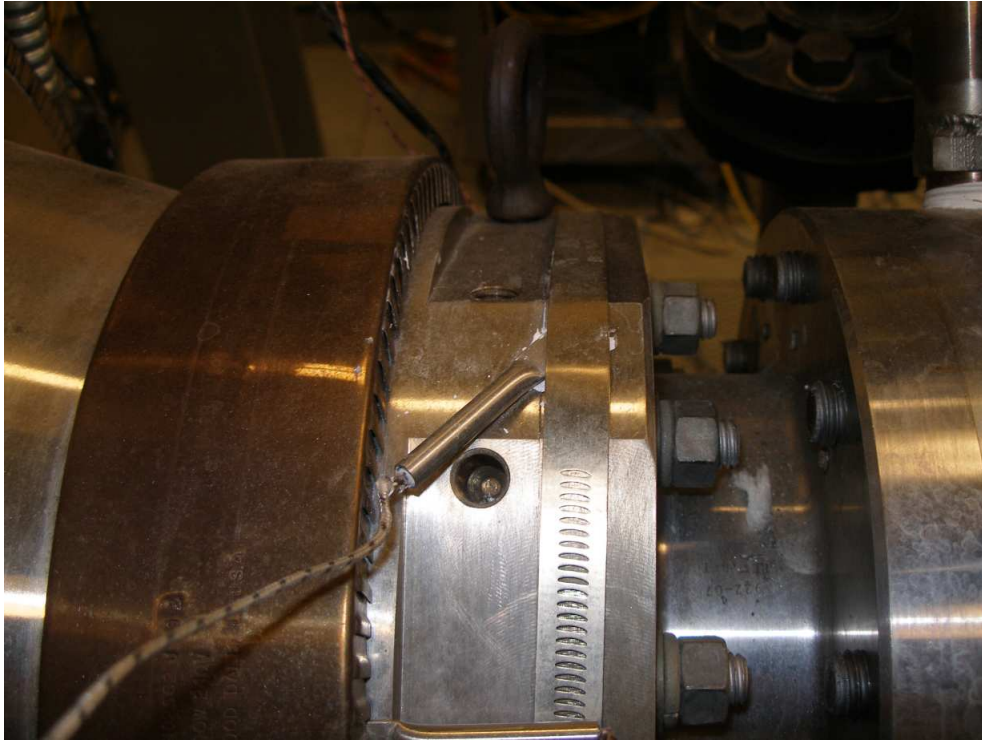
Figure 4.3: Thermocouple used to control contraction heating

It is interesting to note that the temperatures at y_c=6.00 and 8.00 inches are consistently higher than at lower locations. This is evidence that during the equilibrium time between filling the driver tube and running the tunnel the driver tube air stratifies significantly due to temperature variations. If the driver tube walls were well-insulated and uniformly heated, such stratification would not be observed; the air would be at a uniform temperature and no stratification would be observed.

Additionally, the theoretical contraction temperature providing static liquefaction of nitrogen in the exit of the nozzle was computed and plotted for stagnation pressures of 90 and 145 psia. It was found that for 8 psia, the static-liquefaction curve was too far below the observed temperatures to be seen with the current axes and was thus not plotted.

Pope [23] provides the following relation for static nitrogen liquefaction:

$$\log_{10}(p) = \frac{-605.4}{T} + 4.114 \qquad (4.1)$$

where p is in atmospheres and T is in °R. Since the static pressure in the contraction is the nozzle stagnation pressure, the isentropic static pressure was calculated for a Mach number of 5.8. This gave the static pressure in the nozzle exit. The theoretical static temperature providing nitrogen liquefaction was then calculated. The corresponding stagnation temperature was found via isentropic relations. This is what is plotted as the saturation temperature for nitrogen in the nozzle exit.

As can be seen in Figure 4.2, there should be some static nitrogen liquefaction in the nozzle exit for pressures of 90 and 145 psia late into the runs. This is an issue that must be addressed later as such liquefaction is undesirable. However, it is possible that due to the great efforts to remove particulate from the air used to fill the driver tube, supercooling could allow the nitrogen in the air to be cooled below this static-liquefaction point without actually condensing.

Figure 4.4 shows the RMS temperature fluctuations as a percentage of the mean temperature in Kelvin for initial driver-tube pressures of 8, 90, and 145 psia. The three figures could not have the same axes due to the large fluctuations at several points. The RMS was calculated over time periods of 0.01 seconds.

As can be seen, the temperature-fluctuation levels are quite low for all y_c at 8 psia. At 90 and 145 psia, the fluctuations are similarly low from y_c=-3.00 to 2 inches. For values of $y_c > 2$, much larger fluctuation levels, on the order of 0.2% were observed. It is thought that the increased fluctuation levels are due to either convection of nonuniform flow from upstream that develops due to free convection before the run starts or the presence of a thermal boundary layer that develops during a tunnel run. The possible presence of a thermal boundary layer during a tunnel run will be discussed more in depth later in this chapter.
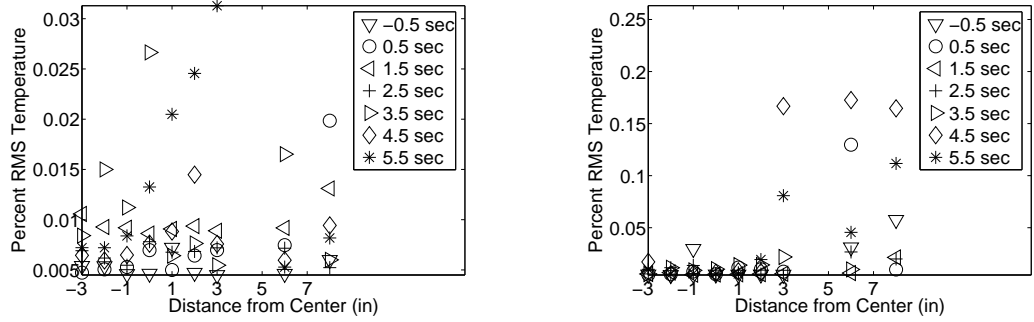
(a) Driver tube initial pressure of 8 psia

(b) Driver tube initial pressure of 90 psia
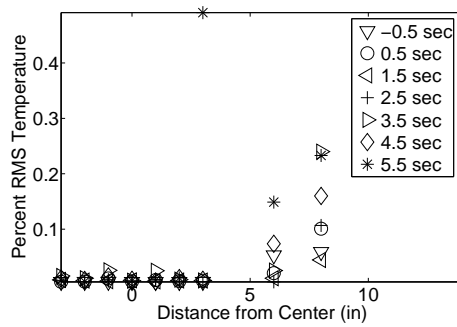
(c) Driver tube initial pressure of 145 psia

Figure 4.4: RMS temperature for full-temperature driver tube at 8, 90, and 145 psia

4.3 Reduced Band-Heater Set Point

In order to mitigate the effect of overheating the contraction, the band-heater set points were reduced and similar measurements were repeated. The previously used wire was positioned very close to the top contraction wall (approximately 0.1 inches). The heaters were all turned down to 120°C.

Runs were made at the same initial driver tube pressures and at locations from y_c=-3.00 to 8.00 inches in 1.00 inch increments. The runs were not made in sequence in order to remove any sort of sequence-dependence. Runs were made in two groups and in the following order: -3.00, 2.00, -2.00, 1.00, -1.00, 0.00 (first group) and 3.00, 8.00, 4.00, 7.00, 5.00, 6.00 inches. The first grouping was completed at 8, 90, and 145 psia respectively. The probe support was then moved up in the traverse to allow
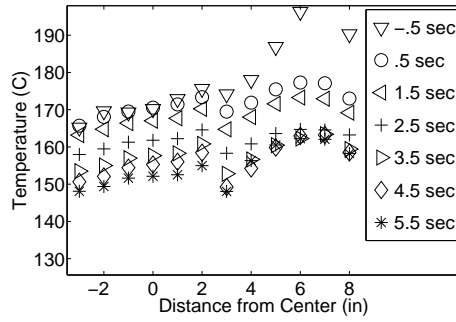
(a) Driver tube initial pressure of 8 psia
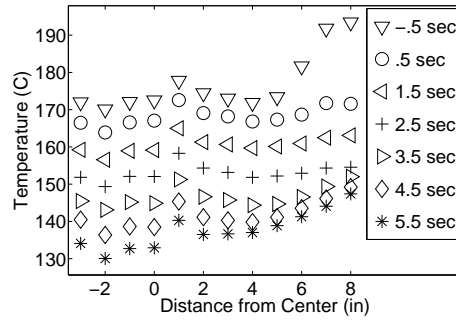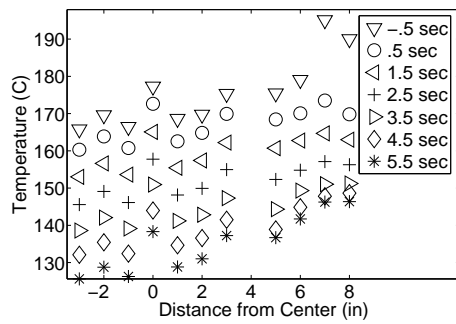
(b) Driver tube initial pressure of 90 psia

(c) Driver tube initial pressure of 145 psia
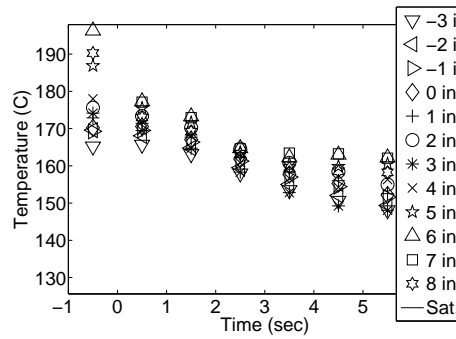
(d) Driver tube initial pressure of 8 psia
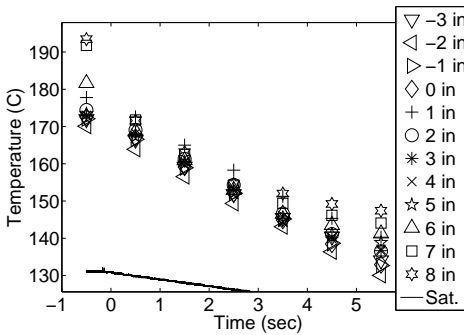
(e) Driver tube initial pressure of 90 psia
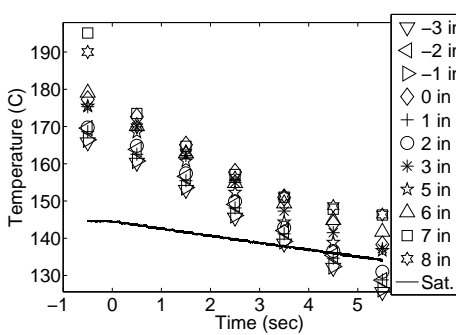
(f) Driver tube initial pressure of 145 psia

Figure 4.5: Temperature profile in contraction with reduced contraction temperature for 8, 90, and 145 psia

the wire to reach the locations in the second grouping. Measurements at the second set of heights were then made for 145, 90, and 8 psia, respectively. These results can be seen in Figure 4.5.

The effect of lowering the contraction temperature is apparent. For the 8 psia cases, the pre-run temperature for locations of -3.00 to 3.00 inches from center remained about the same. The highest pre-run temperature, at a location 6.00 inches above the centerline dropped about 20°C.

For initial pressures of 90 and 145 psia, the pre-run temperatures for locations 6.00 and 8.00 inches above the centerline were also lowered by about 10°C. Surprisingly, however, the pre-run temperatures for locations closer to the centerline were approximately 10°C higher than for the fully heated contraction.

The reason for this unanticipated behavior can be explained by the manner in which the driver-tube temperature is controlled. The thermocouple that reads in the driver-tube temperature to the driver-tube controller is located about 3 feet upstream of the contraction. When the contraction temperature is lowered, the downstream end of the driver tube cools as well. The driver-tube temperature controller then finds the driver tube at a lower temperature and increases the driver-tube temperature accordingly. The elevated driver-tube temperature likely raised the air temperature in the contraction as well, even in the pre-run.

The theoretical saturation stagnation temperature for nitrogen in the nozzle exit is again plotted for the 90 and 145 psia cases. As can be seen, there should theoretically be some nitrogen liquefaction in the nozzle exit for these initial pressures near the end of the run. It should be noted that contraction-air temperature is below this value for less time than for the fully heated contraction. Further study is clearly in order so that nitrogen liquefaction can be avoided.

Figure 4.6 shows the RMS temperature fluctuations as a percentage of the mean temperature in Kelvin for initial driver-tube pressures of 8, 90, and 145 psia for different times during the run. A time of -0.5 seconds is representative of the pre-run fluctuations. The fluctuation levels for the partially heated driver tube and contraction were very similar to those for the fully heated driver tube. Again, for an initial stagnation pressure of 8 psia, the fluctuation levels were very low, on the order of 0.006%. For pressures of 90 and 145 psia, the fluctuations were quite

low for y_c <3.00 inches, but grew to between 0.1% and 0.3% for values greater than 3.00 inches. Although the fluctuation levels are somewhat lower at 145 psia, partially heating the driver tube did not significantly lower RMS temperature fluctuations in the contraction.
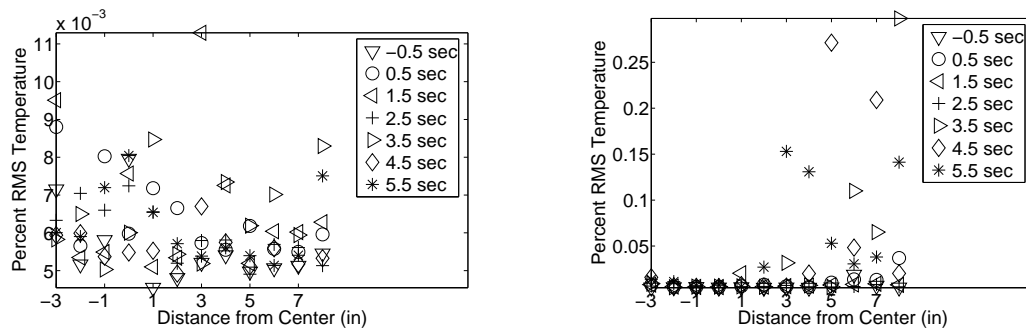
(a) Driver tube initial pressure of 8 psia   (b) Driver tube initial pressure of 90 psia
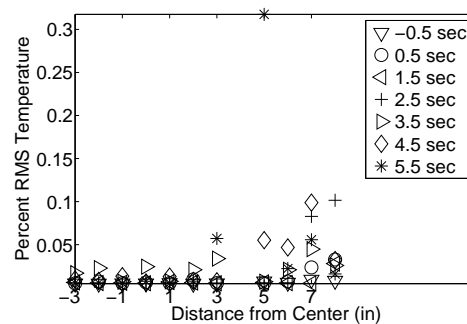
(c) Driver tube initial pressure of 145 psia

Figure 4.6: RMS temperature for partially heated driver tube at 8, 90, and 145 psia

4.4 Temperature Drop Compared to Isentropic Theory

A simple theoretical method for predicting the temporal variation of stagnation temperature and pressure in low Mach-number Ludwieg tubes was developed by Schneider, et al. [24]. The pressure drop is modelled as a simple isentropic expansion from a reservoir through a choked nozzle. The massflow is set by the stagnation temperature and pressure.

The massflow was given by

$$V\frac{d\rho_0}{dt} = -A^*\frac{P_0}{\sqrt{RT_0}}c_1, \tag{4.2}$$

where

$$c_1 = \sqrt{\gamma\left(\frac{2}{\gamma+1}\right)^{\frac{\gamma+1}{\gamma-1}}}, \tag{4.3}$$

A^* is the nozzle throat area, V is the driver-tube volume, T_0 is the stagnation temperature, P_0 is the stagnation pressure, ρ_0 is the stagnation density, and t is time.

For a perfect and isentropic gas,

$$\frac{P_0}{P_{0,i}} = \left(\frac{\rho_0}{\rho_{0,i}}\right)^{\gamma} \tag{4.4}$$

where the subscript "i" denotes initial conditions.

Combining these equations with the perfect-gas relation gave the following as a final relationship for the stagnation pressure ratio drop:

$$\frac{P}{P_0} = \left(1 + \frac{\gamma-1}{2}\frac{A^*}{V}\sqrt{RT_{0,i}}tc_1\right)^{\frac{2\gamma}{1-\gamma}} \tag{4.5}$$

where t is time from the start of the run.

The stagnation-temperature ratio was then easily found from:

$$\frac{T}{T_0} = \left(\frac{P}{P_0}\right)^{\frac{\gamma+1}{\gamma-1}} \tag{4.6}$$

Using these formulas, theoretical temperature ratios were computed and compared to measurements made in the contraction in order to see whether the contraction stagnation temperatures behaved in the same manner as the theory. Figure 4.7 shows these comparisons for the fully heated and the partially heated contraction for initial stagnation pressures of 8, 90, and 145 psia, for the wire locations discussed

above. For all three pressures and both levels of contraction heating, with the exception of the cooler contraction 8 psia runs, locations from -3.00 to 5.00 inches from centerline matched very well with the theoretical, isentropic stagnation-temperature drop.

At around 3.5 seconds into the run, however, the actual stagnation temperature begins to turn up slightly. This varies somewhat from the isentropic theory and is possibly due to the growing displacement thickness which effectively reduces the volume of the tunnel, V in Equation 4.5.

It is clear that there are several locations for which the theory does not come anywhere close to predicting the stagnation-temperature-ratio drop. For the fully heated contraction at initial pressures of 8 and 90 psia, wire locations of $y_c=6.00$ and 8.00 inches showed much lower stagnation temperature ratios for the duration of the runs.

This is most likely due to the high pre-run temperatures observed at $y_c=6.00$ and 8.00 inches. As was previously discussed, these pre-run temperatures were much higher than the temperatures at those locations just 0.5 seconds into the run. This means that the pre-run temperatures measured at $y_c=6.00$ and 8.00 inches are not appropriate to use as T_0.

In order to see if a more accurate initial stagnation temperature could be found for air heated in the driver tube prior to a run, various values of T_0 were used in an attempt to bring the experimental temperature-ratio curve closer to the isentropic theoretical drop. The values of T_0 that brought the curves as close to the theory as possible can be seen in Table 4.1. This was not done for the 8 psia, 120°C contraction case due to the very aberrant behavior of all the curves for this case.

Figure 4.8 shows the stagnation-temperature ratio drop with the modified T_0. As can be seen, all the curves match the isentropic theory much more closely. However, for the cases with the contraction fully heated to 160°C, it is clear that the relationship between the stagnation-temperature ratio and time is characteristically different than the isentropic theory in that it does not have a nearly constant slope.
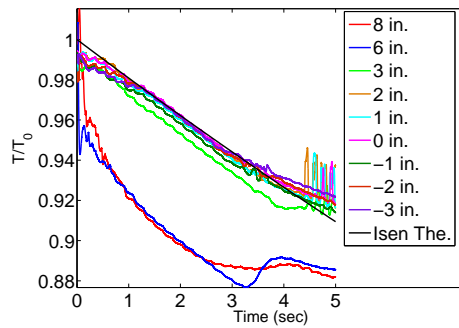
(a) 8 psia, fully heated
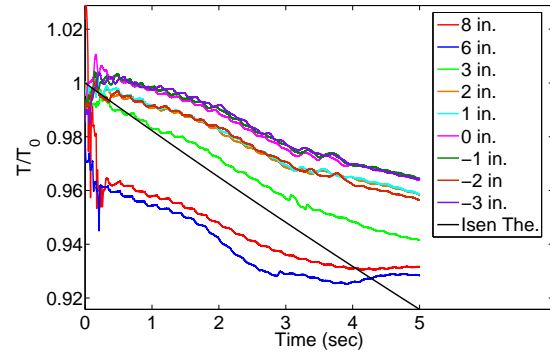
(b) 8 psia, lower temp
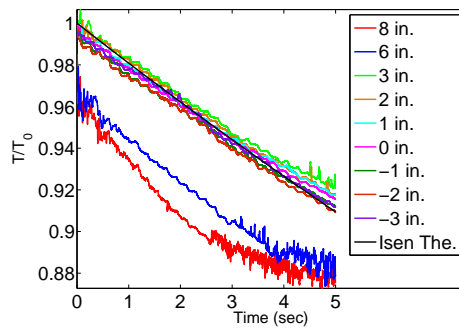
(c) 90 psia, fully heated
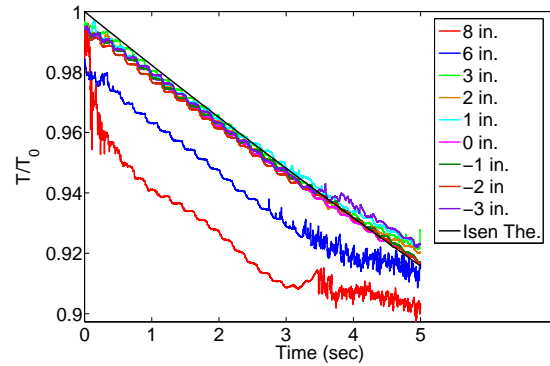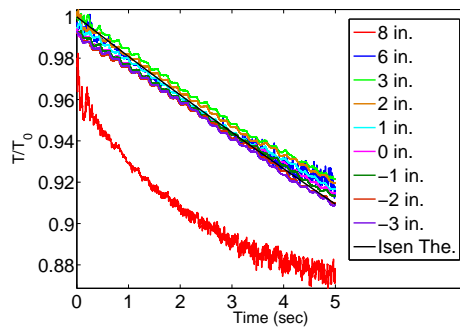
(d) 90 psia, lower temp

(e) 145 psia, fully heated
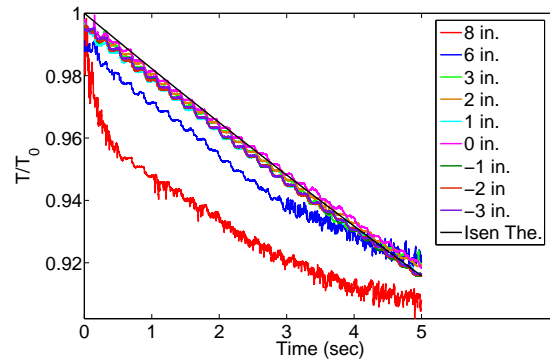
(f) 145 psia, lower temp

Figure 4.7: Contraction stagnation-temperature-ratio drop for 160°C and 120°C contractions, 8, 90, and 145 psia

Contraction Temp	Pressure	T_0 (K) at y_c=8 in	T_0 (K) at y_c=6 in
160°C	8	459	457
	90	451	449
	145	449	442
120°C	90	448	446
	145	449	448

Table 4.1: Different T_0's used to bring temperature ratios closer to isentropic theory

For the 120°C contraction, however, the curves, especially at 90 psia, behave much more like the theory.

The differences between theory and the experimental data are thought to be due to a thermal boundary layer present along the upper tunnel wall during a run. This thermal boundary layer is the portion of the fluid near the wall through which the temperature drops from the wall temperature to the free-stream temperature. Due to the higher contraction-wall temperature, such a thermal boundary layer is expected.

4.5   Comparison with Nozzle Measurements

Additionally, some temperature data were measured in the exit of the Mach-6 nozzle by Shann Rufer [25]. These were compared to both the isentropic theory and the contraction-temperature data. The short run time of the BAM6QT makes the nozzle wall essentially adiabatic. Therefore, the drop in the ratio of stagnation temperature to the initial stagnation temperature should be the same in the contraction and the nozzle exit.

The data collected by Rufer were collected with a hot wire operated in constant-current mode at approximately z=84.4 inches. The wire was platinum/10% rhodium (Pt/Rh). It was 0.00015 inches in diameter with an L/D ratio of approximately 140.

(a) 8 psia, fully heated

(b)

(c) 90 psia, fully heated

(d) 90 psia, lower temp

(e) 145 psia, fully heated

(f) 145 psia, lower temp
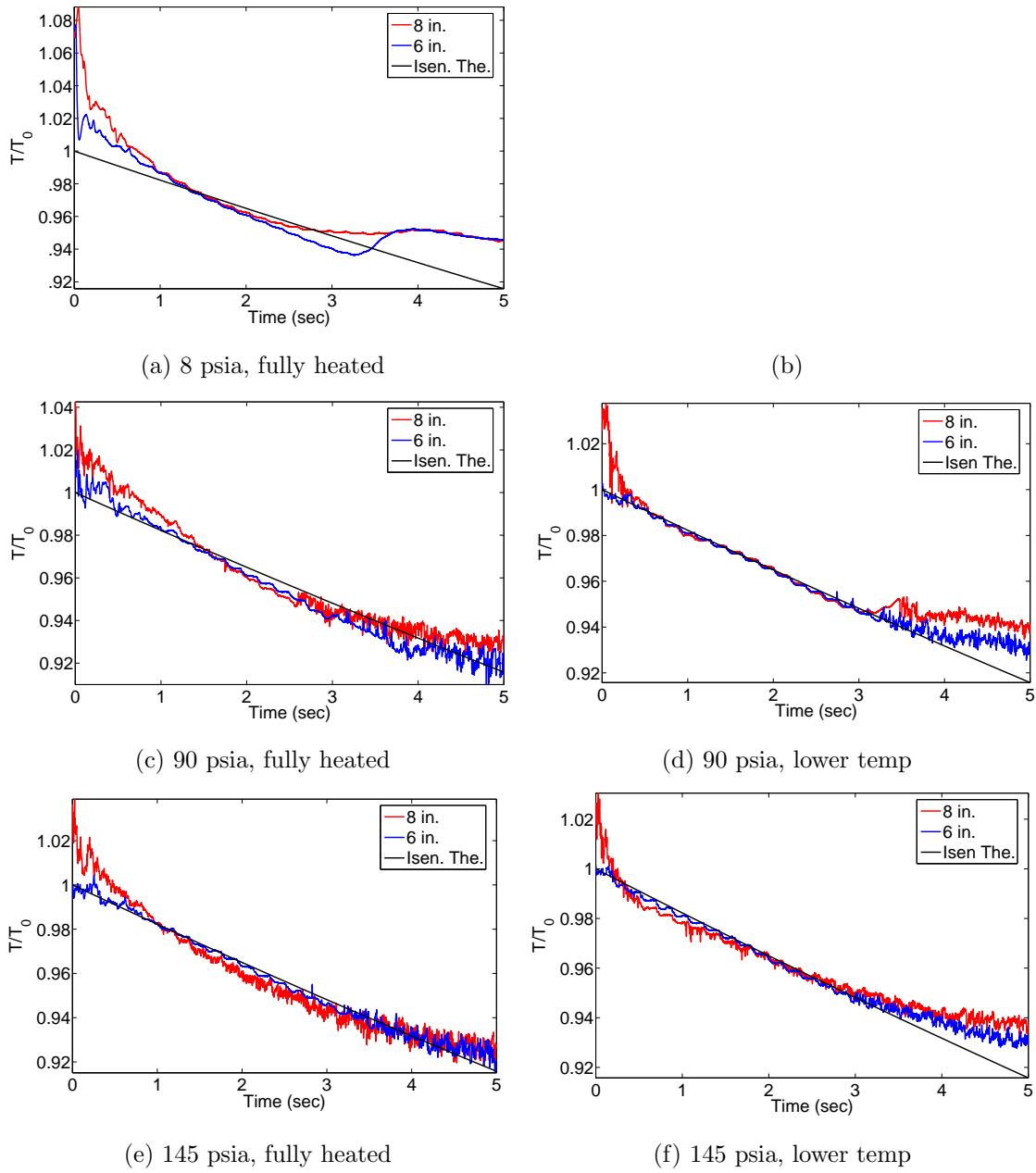
Figure 4.8: Contraction stagnation-temperature-ratio drop for 160°C and 120°C contractions, 8, 90, and 145 psia with prescribed T_0

These data were recorded on the lower resolution LeCroy 9314AL oscilloscope for a 10 second period. This oscilloscope does not have the Hi-Res mode of the Tektronix oscilloscopes. Because of this, data were recorded at a lower sampling frequency than the contraction data recorded on the Tektronix oscilloscope and are more subject to bit noise.

Figure 4.9 shows stagnation-temperature ratios for the fully heated contraction at pressures of 8, 90, and 145 psia, Rufer's data on the tunnel centerline at pressures of 14, 46, 76, 104, and 135 psia, and the isentropic theory. As can be seen, her data lies within about 2% of both the contraction data and the isentropic theory. However, initially there is a significant discrepancy of up to about 4% between her data and the contraction data.

This is probably due to a combination of several factors. First, the denominator of the temperature ratio is taken to be the ideal initial stagnation temperature in the tunnel, 160°C. As has been shown, this is not the true initial stagnation temperature. Secondly, it is likely that the general non-uniform temperature in the contraction affected the stagnation-temperature results in the nozzle exit. Still, there is sufficient agreement to say that the stagnation temperature ratio in the nozzle exit reflects the ratio in the contraction.

Clearly, the temperature distribution in the contraction is very complex. It appears that both a viscous boundary layer and a thermal boundary layer, as well as free convection from the tunnel-wall temperature gradient are all present in the contraction. Some combination of these factors has created an erratic and complicated flowfield which is difficult to model. It is necessary then to determine the effect of these factors and the disturbances they generate on the overall driver-tube noise levels.
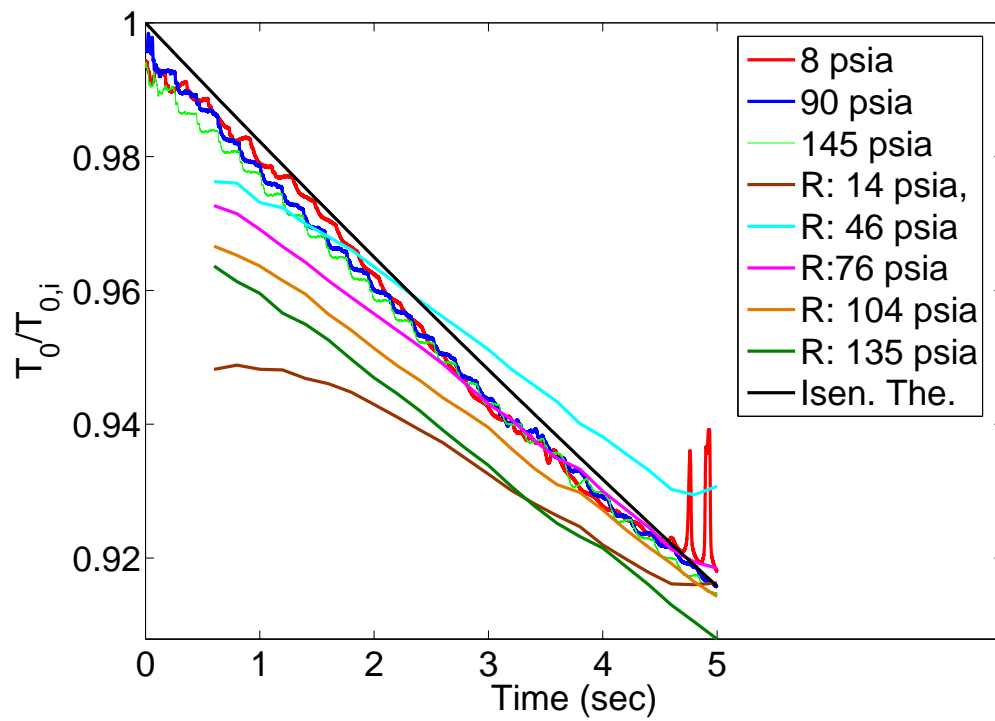
Figure 4.9: Rufer's data compared to contraction data and isentropic theory

5. Hot-Wire Calibration

5.1 Introduction

Free convection due to the temperature gradient present in the contraction wall and driver tube generates a significantly non-uniform temperature profile in the contraction that necessitates an examination of the mass-flow fluctuations. The fluctuations present in the driver tube and contraction could significantly affect freestream noise levels in the nozzle or perhaps create a bypass mechanism that trips the nozzle-wall boundary layer.

A hot wire was chosen as the measurement tool for this task. Due to its small sensor area, a hot wire is capable of resolving mass flow fluctuations on a small area. The high frequency response allows fluctuations on a small time scale to be resolved. A calibration of the hot wire was necessary in order to quantify the disturbances in the contraction. Normally, a calibration of a hot wire in low speed, incompressible flow is a trivial task. However, the changing density due to the passing expansion wave and its reflections in the contraction make this calibration procedure questionable.

A low speed, incompressible hot-wire calibration is normally modelled by King's Law:

$$Nu = A + B\sqrt{Re_w} \qquad (5.1)$$

where A and B are empirical constants, Nu is the Nusselt number, and Re_w is the wire Reynolds number.

As mentioned before, the changing density in the contraction makes it unlikely that this relation is accurate. Thus, a new calibration procedure was established and performed. Additionally, the same data were used in another previously established

calibration scheme. Mass-flow fluctuations computed from both calibrations were then compared.

For the present study, no contraction boundary-layer effects were considered. As will be discussed in detail in Chapter 7, the boundary layer in the contraction is highly complex and asymmetric. This makes modelling it in the calibration very difficult. The displacement thickness of the viscous boundary layer would serve to raise the contraction Mach-number. It seems likely that a change in Mach number would affect the calibration. No doubt this exclusion added some error and uncertainty to the calibration. However, at present, it seems the only way to proceed.

5.2 Calculation of Mass Flow

Both calibration procedures require the mass flow to be known. A relationship between the output of a static-pressure transducer and the mass flow can be easily derived (see Nomenclature section for symbol definitions). A simple equation for mass flow is:

$$\dot{m} = \rho U A_C \tag{5.2}$$

From the perfect gas law:

$$\rho = \frac{P}{RT} \tag{5.3}$$

U can be expressed as:

$$U = M\sqrt{\gamma RT} \tag{5.4}$$

By combining Equations 5.2-5.4 the following expression is obtained:

$$\rho U A_c = \frac{P}{RT}M\sqrt{\gamma RT}A_c \tag{5.5}$$

Simplifying Eq. 5.5 yields:

$$\rho U = PM \sqrt{\frac{\gamma}{RT}} \qquad (5.6)$$

The contraction-entrance Mach number was found using the isentropic area relationship where the cross-sectional area of the contraction was taken to be 238.1 square inches and the throat area was taken to be 1.7 square inches. This value of the throat area is 1.38 times the geometric throat area to account for the additional area due to bleed-slot suction. Due to the low Mach number, about 0.004, the stagnation and static temperatures are essentially identical at the driver-tube exit. Thus Eq. 5.6 can be used as the final equation for mass flow.

The static pressure in the contraction, P in Equation 5.6, was found from the calibrated Kulite static-pressure transducer located on the contraction wall. The sensor was calibrated by first opening the gate valve until the pressure had dropped to low vacuum, about 0.2 psia. The gate valve was closed. The air in the tunnel was allowed to equilibrate. Then the conditioned output voltage of the transducer was recorded along with the tunnel pressure, measured by the Paroscientific gauge. The tunnel pressure was then pressurized to approximately 145 psia in incremental steps. At each step, the air was allowed to equilibrate and voltage and pressure levels were recorded.

Figure 5.1 shows a typical calibration for the contraction Kulite. As expected, the voltage-pressure relationship was very linear. This calibration procedure was completed regularly to ensure that the calibration had not shifted and that the sensor had not gone bad.

5.3   Calibration Method 1

The goal of this first calibration procedure was to find a relationship between Nusselt number and Reynolds number valid over the entire range of contraction conditions. This could then be compared to the standard King's Law relationship
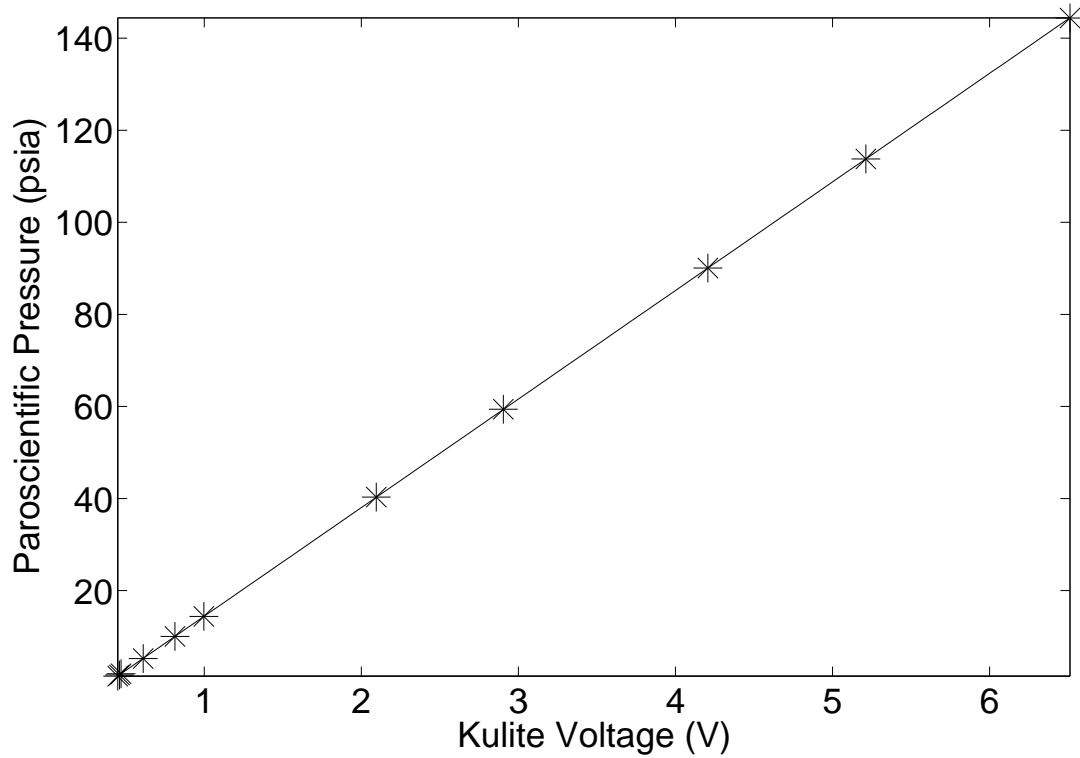
Figure 5.1: Contraction static-pressure transducer calibration

for low-speed incompressible flow. It was thought that the relation would be of the form:

$$Nu = CRe_w^n \qquad (5.7)$$

with C and n being empirical constants determined in the calibration.

The Nusselt number is given by

$$Nu = \frac{E^2 R_w}{\pi kl(T_w - \eta T_0)(R_a + R_w)^2} \qquad (5.8)$$

Due to the low-speed flow, η can again be taken to be 1 [20]. Variables are defined in the Nomenclature section.

For calibration purposes, the wire Reynolds number is given by

$$Re_w = \frac{\dot{m}d}{\mu} \tag{5.9}$$

where $\dot{m}$ is known from Equation 5.6.

An analytical expression of the mass flow fluctuations computed from this calibration procedure was found. Combining Equations 5.7 and 5.8 gives:

$$\frac{E^2 R_w}{\pi kl(T_w - T_0)(R_a + R_w)^2} = CRe_w^n \tag{5.10}$$

Substituting Equation 5.9 and solving for mass flow (in the Reynolds number) gives:

$$\rho u = \frac{\mu}{d}\left(\frac{E^2 R_w}{C\pi kl(T_w - T_0)(R_a + R_w)^2}\right)^{1/n} \tag{5.11}$$

Assuming that a fluctuation in the mass flow will be evidenced by a corresponding fluctuation in voltage, the following can be stated:

$$\frac{\overline{\rho u} + \widetilde{\rho u}}{\overline{\rho u}} = \frac{\frac{\mu}{d}\left(\frac{(\overline{E}+\widetilde{E})^2 R_w}{C\pi kl(T_w - T_0)(R_a + R_w)^2}\right)^{1/n}}{\frac{\mu}{d}\left(\frac{\overline{E}^2 R_w}{C\pi kl(T_w - T_0)(R_a + R_w)^2}\right)^{1/n}} \tag{5.12}$$

where a barred quantity represents a mean value and tilde represents some perturbation from the mean. Simplifying and rearranging gives:

$$\frac{\widetilde{\rho u}}{\overline{\rho u}} = \left(1 + \frac{\widetilde{E}}{\overline{E}}\right)^{2/n} - 1 \tag{5.13}$$

Equation 5.13 can be approximated using the first two terms of a binomial expansion:

$$\frac{\widetilde{\rho U}}{\overline{\rho U}} \approx \frac{2}{n}\frac{\widetilde{E}}{\overline{E}} \tag{5.14}$$

Thus the fluctuation levels calculated using this calibration scale with $\frac{1}{n}$. Clearly, the fluctuation levels will be very dependent on the value of n found in fitting the data. The closer n is to 0, the larger the calculated fluctuations will be. Interestingly, the fluctuation levels do not depend on the value C at all.

5.3.1   Preliminary Calibration: Assumption of Constant Temperature

In order to calibrate the hot wire for the changing density conditions, calibration runs were completed with different initial stagnation pressures, providing a variety of Reynolds numbers. Calibration runs with initial stagnation pressures of 15, 30, 45, 75, 90, 105, 120, 135, and 140 psia were conducted.

Additionally, at each pressure, one run was made utilizing the active bleed suction and one was made with the bleeds closed. This provided different Mach numbers in the contraction. The open bleeds increased total mass flow by approximately 38%, thus increasing the effective throat area by 38%. This changed the driver tube inviscid, isentropic Mach number from about 0.00292 to 0.00403. For the bleeds open case, the same contraction and throat cross-sectional areas were used as before. For the bleeds closed case, the contraction area was again taken to be 238.1 square inches. The throat area was taken to be the geometric area, 1.2 square inches.

The hot-wire probe was placed along the centerline of the tunnel perpendicular to the direction of air flow. After the tunnel was pressurized to the desired initial stagnation pressure, the air was allowed to equilibrate for approximately 10 minutes before a run was initiated. This time period was chosen because 10 minutes is the standard equilibration time for the BAM6QT as determined in Reference [12]. After each run, the data were saved.

In order avoid the effect of the passing expansion wave and to ascertain the effect of time and pressure change on the calibration, calibration calculations were made during three different quasi-static periods between expansion wave reflections for each run. Calibration calculations were made after the third, seventh, and twelfth reflections. Average values were calculated over 0.25 seconds.

In the calculation of Nusselt number, the temperature was taken to be a constant 160°C. The viscosity and thermal conductivity were then constant values based on the 160°C constant temperature. This is obviously inaccurate since the contraction air, even on centerline, is not always 160°C. More importantly, the expansion wave

serves to lower the temperature as it passes. At the time of these measurements, the capability of inserting multiple probes into the contraction in order to obtain simultaneous temperature measurements did not exist. Because of this inhibition, the temperature was taken to be constant.

The expansion-wave period is approximately 200 milliseconds. Since the active bleed valve opens about 1 second after the start of a run, bleed suction was never present for the period after the third expansion-wave reflection. For the periods after the seventh and twelfth waves, data were collected both with and without bleed suction.

Figure 5.2 shows the results of a set of calibration runs. Mass flow is plotted against the square of hot-wire voltage. Nusselt number is also plotted against wire Reynolds number. As can be seen, all the calibration curves calculated for runs with the bleeds closed matched quite nicely. In both plots, the data using the bleed system is offset from the data with no suction. At worst, it is about 10% below the no-bleeds case. It seems that calibrating with a different contraction Mach number creates an undesirable change in the calibration. This could be due to an inaccurate contraction Mach number for the closed bleed condition because of an unsteady flow separation over the bleed lip. Such an unsteady separation would cause the effective throat area to fluctuate and thus cause the contraction Mach-number to fluctuate as well. This possibility can neither be verified nor dismissed. Because of this fact and because the tunnel must use the bleed system to run quietly, subsequent calibrations used the bleed system for all runs. From these limited data, it appeared that calibrating at a different time or pressure had little effect on the calibration.

5.3.2   Preliminary Calibration: Changing Temperature

The experimental setup was modified by inserting another hot-wire probe through the 3-inch instrument port on the bottom of the contraction, at the same axial location as the top port. In the same manner as the top wire, this wire was held

(a) Mass flow vs. square of hot-wire voltage

(b) Nu vs. Re_w
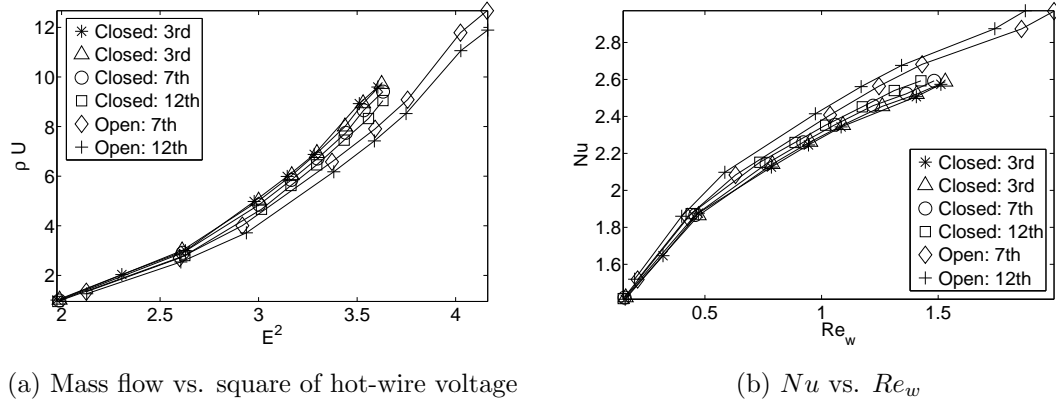
Figure 5.2: Calibration runs with and without bleed suction on different expansion wave reflections

in a probe support which was affixed to a traverse. This allowed precise vertical positioning of the probe.

A series of tunnel runs were completed in order to ascertain the minimum distance between probes to avoid interference due to the proximity of the other wire. First, the top wire, connected to the CTA, was located on the tunnel centerline. The bottom wire, connected to the CCA, was then positioned 6.00, 0.25, 0.18, and 0.10 inches below the top wire. Runs were made at 45 psia. The bottom wire was then positioned on the centerline and the top wire was located 5.00, 1.00, 0.25, and 0.10 inches above the wire. Runs were again made at 45 psia.

The signal from the wire located on the centerline was examined. The RMS of the signal was calculated for periods of 0.01 seconds over the 1.0 second of pre-run data and over the 6.0 seconds of run data. The RMS levels for different probe spacings were compared to see if there was an effect.

Figure 5.3 shows the RMS of the top-wire voltage trace for different probe spacings for the case with the top wire, operating in constant-temperature mode, on centerline where the bottom wire, operating in constant-current mode, position was varied. Here, for the sake of clarity, only every 10th point is shown. The data with

the bottom wire stationary on the tunnel centerline with varying top-wire position looked much the same.

It is not clear that any of the spacings examined actually caused a change in the RMS signal from the other wire. The RMS, due to both electrical noise and any mass-flow disturbances in the contraction, behaved similarly for all the different probe spacings that were examined. The RMS associated with a spacing of 6.00 inches was much the same as that with a spacing of 0.10 inches. Therefore, it can be concluded that any spacing, down to 0.10 inches, would not cause interference. Nevertheless, to ensure that there would be no interference, a spacing of 0.18 inches was used for subsequent measurements.
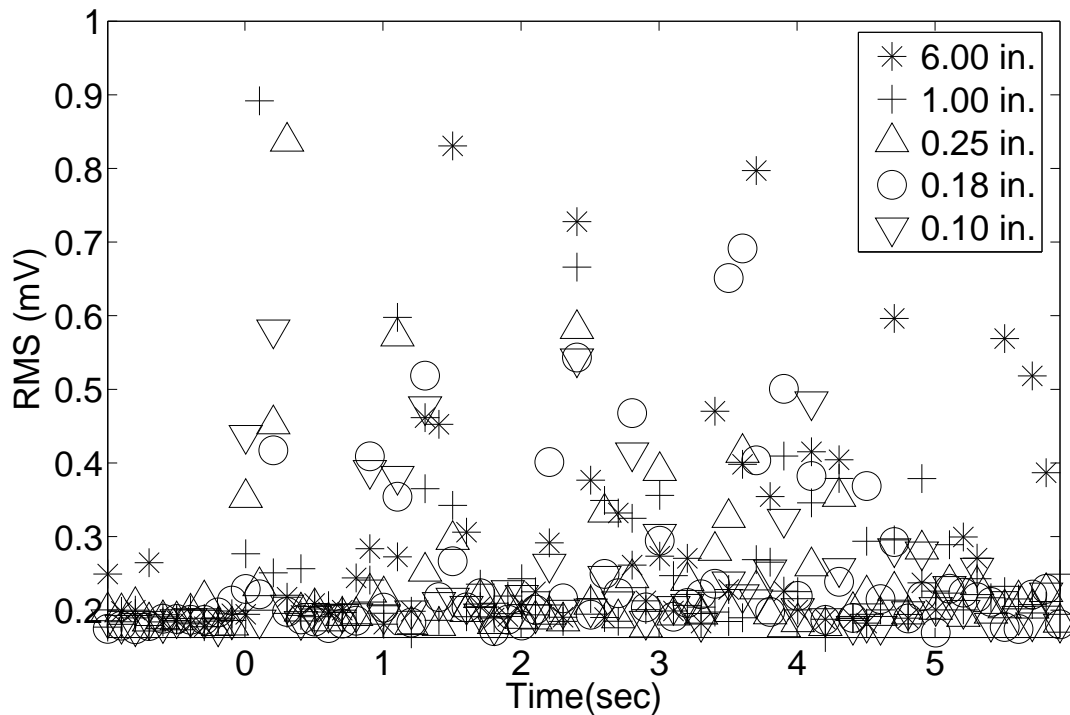
Figure 5.3: RMS for changing bottom-wire location

Runs with two wires in the contraction were made for initial stagnation pressures of 8, 15, 25, 35, 45, 65, 90, 105, 125, and 140 psia. These pressures were chosen

because over the course of these 6 second runs, almost every pressure between 6 and 140 psia was reached by at least one run. The order in which the initial pressures were run was different than this list, however, in order to remove any sort of dependence on the sequential pressure change. The wire connected to the CTA was positioned on the centerline. The temperature-sensing wire was positioned 0.18 inches below this.

Instead of calibrating the wire based on the data after just one expansion-wave reflection as before, the entire run was broken up into smaller periods of length Δt. Each of these periods was used as a data point for finding a calibration relationship for the wire.

With the addition of the temperature-sensing wire, the actual values of a number of variables previously taken to be constant could be calculated. Temperature, viscosity, and the thermal conductivity of air all became changing quantities.

The flow temperature was directly sensed by the wire connected to the CCA. The thermal conductivity of the air in the contraction was then calculated from Sutherland's thermal conductivity relation [26]:

$$k = 0.0241 \left(\frac{T}{273} \right)^{\frac{3}{2}} \frac{467}{T + 194} \tag{5.15}$$

Viscosity was found from Sutherland's viscosity law [26]:

$$\mu = 0.00001716 \left(\left(\frac{T}{273} \right)^{\frac{3}{2}} \frac{384}{T + 111} \right) \tag{5.16}$$

In both cases, units are MKS. The collected data were used to compute many Nu-Re_w data points. A non-linear least-squares solver in Mathematica was used to fit the data by finding the best C and n of Equation 5.7 to fit the data.

Figure 5.4 shows the difference between using the constant temperature assumption and using the true temperature. Figure 5.4a shows the Nusselt number vs. Reynolds number for constant temperature, thermal conductivity, and viscosity. Figure 5.4b shows the same thing but with temperature, thermal conductivity, and viscosity changing.

(a) Nu vs. Re_w, assuming constant T

(b) Nu vs. Re_w, changing T
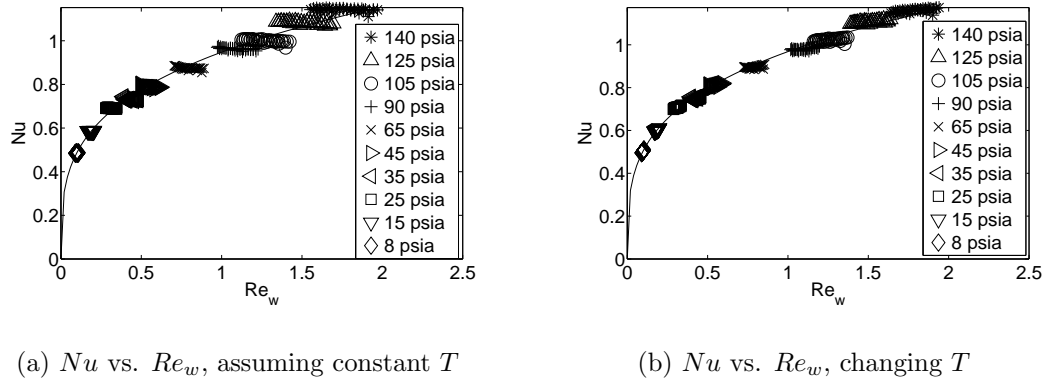
Figure 5.4: Nu vs. Re_w with constant and changing temperature

There is a very noticeable difference between the two figures. As can be seen, in the case with changing temperature, the data do not collapse entirely, but they are much closer to the power curve fit than for the constant temperature case. The constant-temperature case gave a Nusselt number/Reynolds number relation of

$$Nu = 0.948 Re_w^{0.288} \tag{5.17}$$

while the changing-temperature case gave

$$Nu = 0.970 Re_w^{0.286} \tag{5.18}$$

Although the curve fits are very close, the one found with changing temperature most closely represents the conditions in the contraction. This calibration method was therefore used for the calculation of mass-flow fluctuations.

As was mentioned before, the mass-flow fluctuations computed from this calibration procedure will scale with a function of the hot-wire mean and fluctuating voltages raised to $\frac{2}{n}$ (Equation 5.13). It is essential to examine the change in n for a range of Δt's to ensure that the value of n is not based on this parameter. Additionally, the extent to which the calculated C and n give the best fit of the data must be examined.

The same data were processed for different Δt's. The computed curve-fit parameters are shown in Table 5.1. As can be seen, for Δt ranging from 0.005 to 0.500 seconds, there is only about a 0.1% change in n. This demonstrates that the value of n is not very dependent on the value of Δt.

Δt	C	n
0.500	0.971786	0.285257
0.200	0.970180	0.285528
0.100	0.970182	0.285529
0.050	0.969938	0.28556
0.020	0.969792	0.285574
0.010	0.969744	0.285579
0.005	0.969721	0.285583

Table 5.1: Calibration constants calculated for different Δt's

A Δt of 0.01 seconds was chosen because it gave a reasonable number of data points over which to average. It has been shown that the period of the reflecting expansion wave in the driver tube is approximately 200 ms. If the chosen Δt were too large, many of the aforementioned time periods would include the quasi-static pressure, temperature, and density drop associated with the passing expansion wave. This would skew the mean value for that time period and also introduce a higher RMS. With a Δt of 0.01 seconds, only about 1 in every 20 time periods spanned a passing expansion wave, thus minimizing the effect of the wave.

In order to gain a better understanding of the calibration parameters, it was useful to make a plot in $C - n$ space of how unique the calculated calibration constants were. For a given Δt, Nusselt number and Reynolds number were computed for all calibration data. These values were input into a MatLab code which varied C and n over a prescribed range. A correlation coefficient, R^2, for a linear relationship

between the the right and left sides of Equation 5.7, was calculated. A value of 1 corresponds to an exact fit with values less than 1 being a worse fit. A sample contour plot of R^2 in $C - n$ space for $\Delta t = 0.010$ is shown in Figure 5.5.
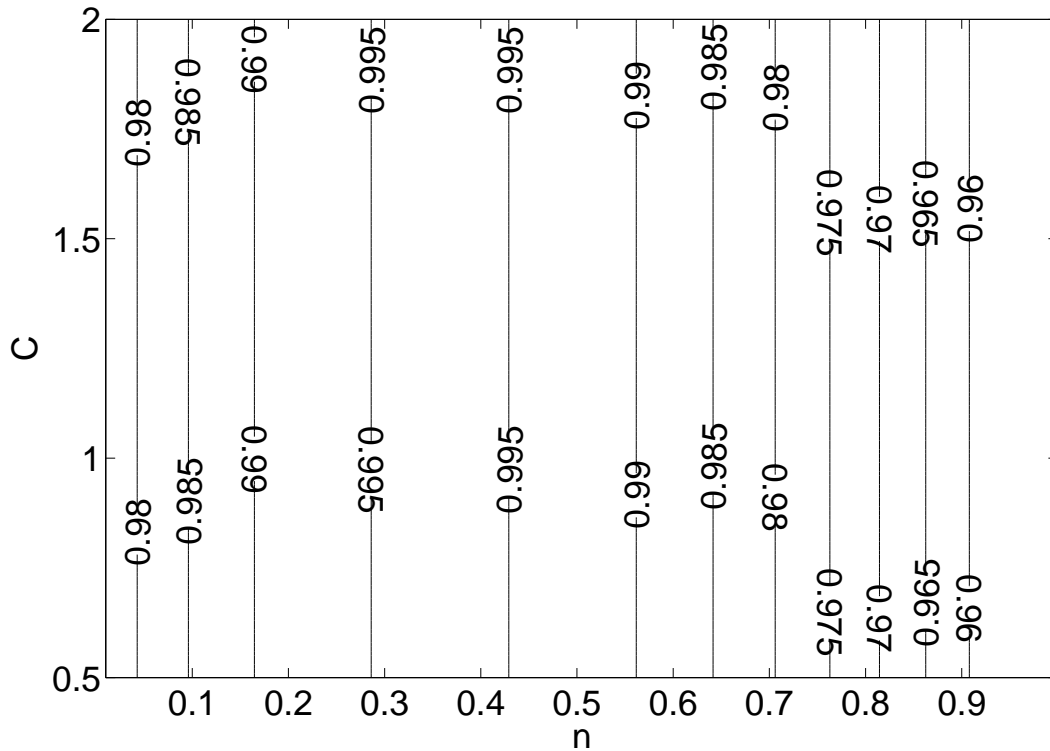
Figure 5.5: R^2 contour plot in $C - n$ space

As can be seen, there are apparently many values of C that give a good fit. However, there is only one value of n that gives the highest R^2 value on the plot. This shows that the particular n found in the non-linear least-squares fit really is the best n possible. This fact, combined with the consistency of n and C found with different Δt's provide compelling evidence that this calibration technique will provide reliable mass-flow fluctuations.

5.4   Calibration Method 2

The calibration procedure described in Section 5.3 seemed to make sense and take the changing temperature and density present in the contraction flow into account. Nevertheless, finding an established calibration method for this type of flow with which to compare it was thought to be a good idea.

A hot-wire calibration for similar flow conditions was found. The calibration relation is taken from Miley and Horstmann [27, 28] and is as follows:

$$A + B\frac{E^2}{k_f(T_w - T_e)} = Re_f^a \sigma^b \tag{5.19}$$

where A, B, a, and b are constants found from a non-linear least squares fit of the data, E is the hot-wire voltage, k is the thermal conductivity, T_w is the wire temperature, T_e is the air temperature, Re is Reynolds number based on wire diameter, and σ is the sea-level air-density-ratio. The subscript "f" denotes quantities found at film conditions, defined as the average temperature of the wire and the surrounding fluid.

Miley used this relation to calibrate a hot wire using data collected both in ground facilities and also from a small low-speed airplane flying at different altitudes. The use of airplane data provided an environment of incompressible flow, but with different temperatures and densities. The conditions in the contraction entrance are very similar to this. Miley's data from ground tests and airplane tests collapsed nicely using Equation 5.19.

This calibration technique was also studied in order to affirm its validity for present experimentation. An analytic analysis of the mass flow fluctuations was again performed to determine the sensitivity to changes in the empirical parameters.

Rearranging Eq. 5.19 and using the definition of the Reynolds number yields

$$\rho U = \frac{\mu}{d}\left(\frac{A + B\frac{E^2}{k_f(T_w - T_e)}}{\sigma^b}\right)^{1/a} \tag{5.20}$$

where ρU is the mass flow, d is the wire diameter, and μ is the viscosity of air at the film temperature.

An analytic solution of the ratio of mass-flow fluctuations to the mean was found utilizing Eq. 5.20. Assuming again that mass-flow fluctuations would be evidenced by a corresponding hot-wire voltage fluctuation, the following can be stated:

$$\frac{A + \frac{B(\overline{E}+\widetilde{E})^2}{k_f(T_w - T_e)}}{A + \frac{B\overline{E}^2}{k_f(T_w - T_e)}} = \frac{\left(\frac{(\overline{\rho U}+\widetilde{\rho U})d}{\mu}\right)^a \sigma^b}{\left(\frac{\overline{\rho U}d}{\mu}\right)^a \sigma^b} \tag{5.21}$$

where variables with a tilde represent perturbation values and those with a solid line represent a mean value. Simplifying, and rearranging gives a solution for the mass flow fluctuations:

$$\frac{\widetilde{\rho U}}{\overline{\rho U}} = \left(\frac{Ak_f(T_w - T_e) + B(\overline{E}+\widetilde{E})^2}{Ak_f(T_w - T_e) + B\overline{E}^2}\right)^{1/a} - 1 \tag{5.22}$$

The $(\overline{E}+\widetilde{E})^2$ term can be expanded. In the result, $\widetilde{E}^2$ is ignored since it is assumed that $\overline{E} >> \widetilde{E}$. Further simplification gives a final expression of mass flow fluctuations as

$$\frac{\widetilde{\rho U}}{\overline{\rho U}} = \left(1 + \frac{2B\overline{E}\widetilde{E}}{Ak_f(T_w - T_e) + B\overline{E}^2}\right)^{1/a} - 1 \tag{5.23}$$

Using the first two terms of a binomial expansion, the fluctuation levels can be approximated by:

$$\frac{\widetilde{\rho U}}{\overline{\rho U}} \approx \frac{1}{a}\frac{2B\overline{E}\widetilde{E}}{Ak_f(T_w - T_e) + B\overline{E}^2} \tag{5.24}$$

Clearly, there is no explicit dependence upon b in the mass flow fluctuations. The fluctuations do, however, scale by $\frac{1}{a}$. This means that the closer a is to zero, the larger the mass flow fluctuations would be for the same voltage fluctuations. The determination and consistency of a calculated from the calibration data is of the utmost importance.

In order to ensure that the calibration took into consideration all the flow conditions, each calibration run was broken up into a number of small time periods, Δt.

For each of these time periods, ρU, E, T, σ, and k_f were all calculated. Mass flow, ρU, was found in the same manner as that in Section 5.3, and T was found as before.

With each of these quantities determined, a Mathematica code similar to that used for the other calibration analysis was used to find a nonlinear least-squares fit of the data by solving for the calibration constants, a, b, A, and B in Equation 5.19. Since it is clear that the calculated mass-flow fluctuations will depend largely on the value of a calculated in the calibration, a series of different Δt's were again tried to examine the variation in the calibration constants due to this parameter. Table 5.2 shows the values of these constants based on the chosen Δt. Although the values are all close to one another, there was still about an 11% change between $\Delta t = 0.500$ and $\Delta t = 0.005$

Δt	a	b	A	B
0.500	-0.141966	0.484144	-0.311254	14.5246
0.200	-0.131613	0.477216	-0.323539	14.4713
0.100	-0.131761	0.477365	-0.323604	14.4744
0.050	-0.123188	0.469548	-0.323180	14.3294
0.020	-0.118183	0.465019	-0.323117	14.2474
0.010	-0.116806	0.463811	-0.323274	14.2266
0.005	-0.116095	0.463190	-0.323363	14.2160

Table 5.2: Calibration constants calculated for different Δt's

Figure 5.6 shows how the calibration data collapsed using the calibration constants associated with a Δt of 0.010 seconds. The overall fit is quite good, though there is some deviation from the curve fit. Since it was the best fit, it was used in subsequent calculations of fluctuation levels.

In the course of understanding the intricacies of this calibration, it was found that there is not one clearly best a/b combination. In fact, very different values of
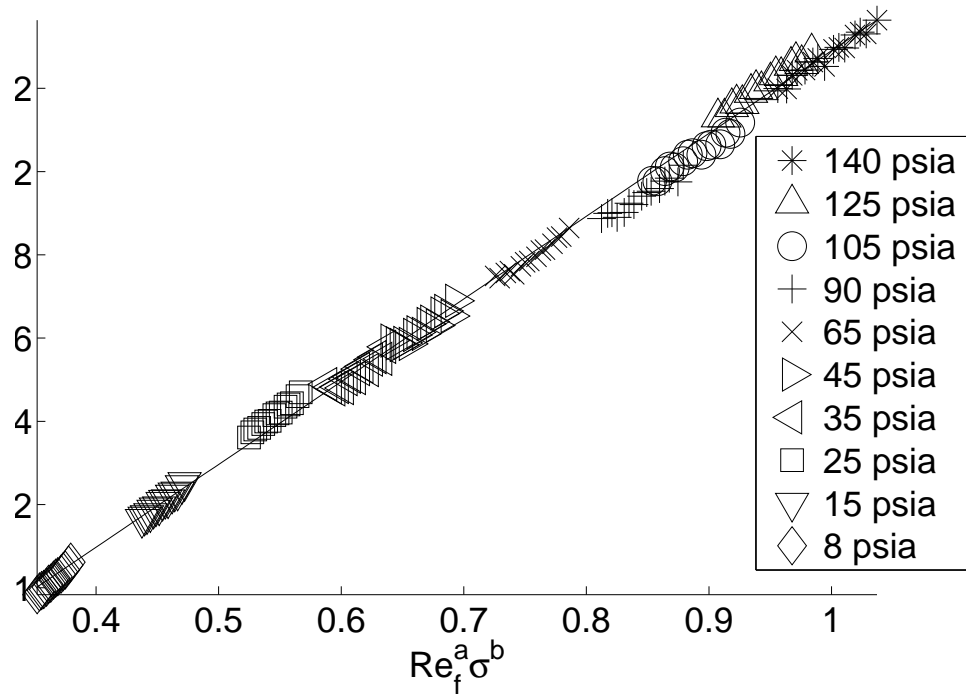
Figure 5.6: Collapse of calibrated data for $\Delta t = 0.010$ sec

a and b collapsed the data nicely. In order to gain a better understanding of the calibration parameters, it was useful to make a plot similar to Figure 5.5 in $a - b$ space. For a given Δt, Reynolds number, sea-level density-ratio, and the left hand side of Equation 5.19 were computed for all calibration data. The left-hand-side term did not include A and B as they are just the slope and intercept implicit in a plot of $\frac{E^2}{k_f(T_w - T_e)}$ vs. $Re_f^a \sigma^b$.

These values were input into a MatLab code which varied a and b and computed the right hand side of Equation 5.19. Again, the correlation coefficient, R^2, was computed. A sample contour plot of R^2 in $a - b$ space for $\Delta t = 0.500$ is shown in Figure 5.7.
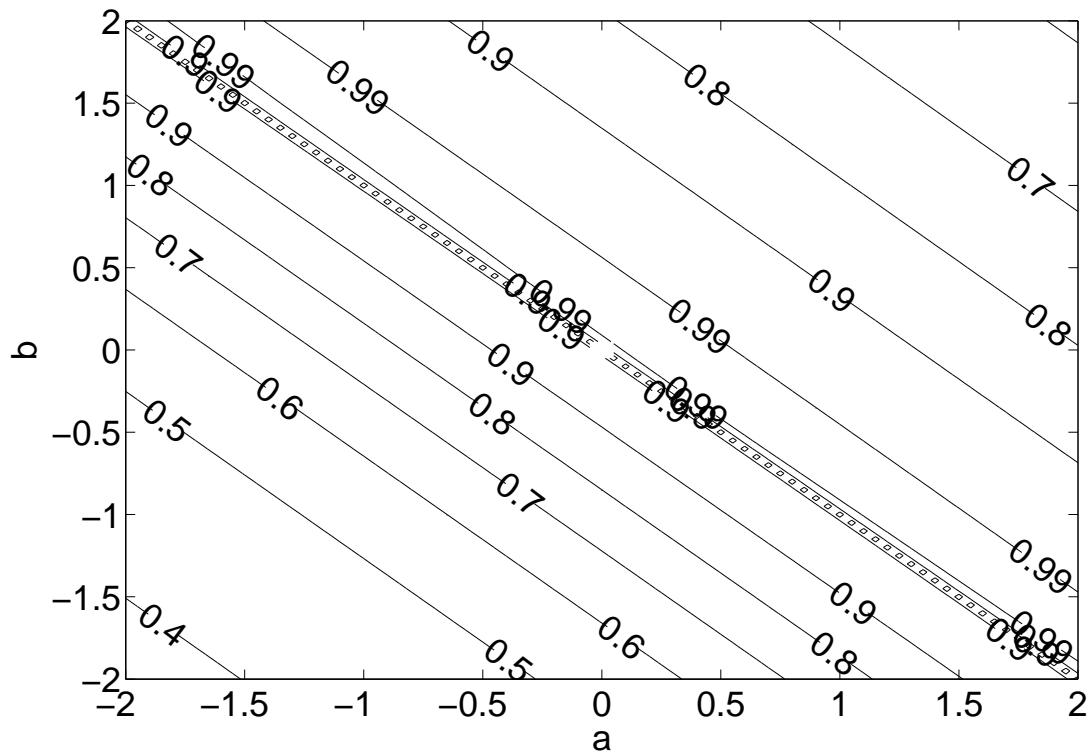
Figure 5.7: R^2 contour plot in $a - b$ space

It is clear from the large swath of $R^2 > .99$ in Figure 5.7 that there are a wide variety of a/b combinations that provide a very good fit of the data. Figure 5.8 further supports this by showing how the data collapse quite well with a very different a/b combination. Here, a is 0.577 and b is -0.229. This gave an R^2 of approximately 0.998. The data do not collapse quite as well as for the calculated calibration constants. Nonetheless, this discrepancy makes this calibration procedure questionable at best. With the mass flow fluctuations being so sensitive to the value of a, a being so sensitive to Δt, and such a wide variety of a/b combinations providing a good fit of the data, the actual mass flow fluctuations found with this procedure will be in doubt.
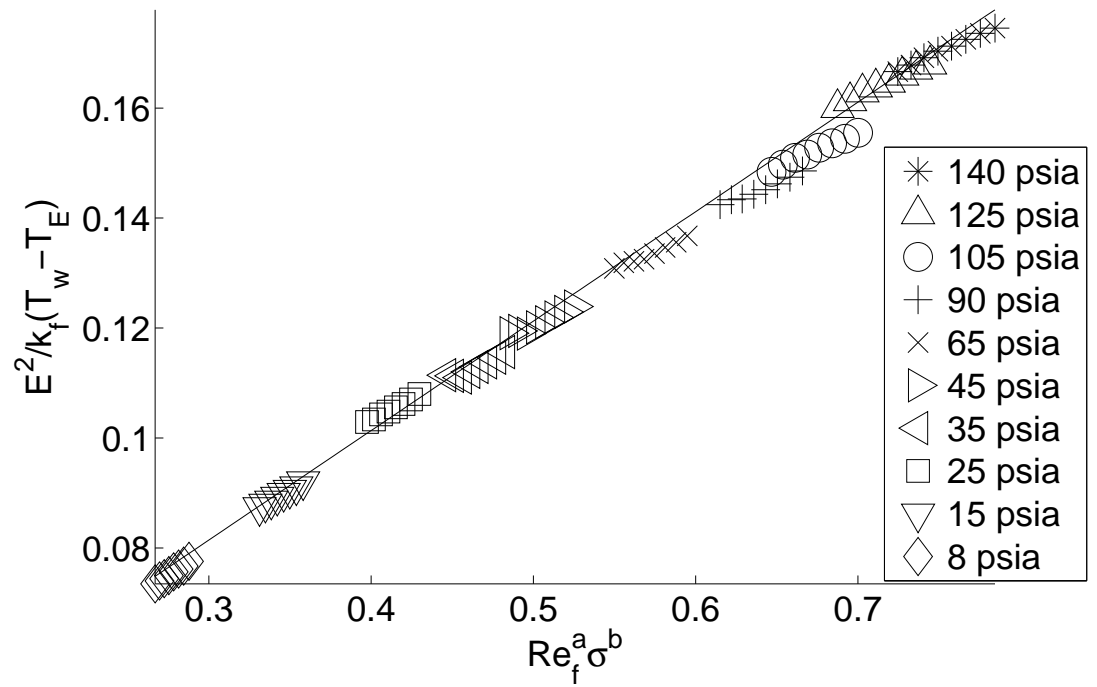
Figure 5.8: Collapse of calibrated data for arbitrary a and b that gave high R^2

6. Mass-Flow Fluctuations

6.1 RMS Fluctuations in the Driver Tube

With a calibrated hot wire, the mass-flow fluctuations in the contraction could be easily measured. Mass-flow fluctuation levels were found for y_c=-6.00, -3.00, 0.00, 3.00, and 6.00 inches. Fluctuation levels were calculated with both calibrations in order to compare the results. As before, data were sampled at 200kHz in Hi-Res mode.

The hot-wire oscilloscope trace from a particular run was converted into mass flow via the calibrations. Both calibrations have a term which is the Reynolds number raised to a power. The Reynolds number was broken up into the mass flow and the quantity $\frac{d}{\mu}$. All quantities other than the mass flow were known. Thus, mass flow was inferred from the Reynolds number for each calibration.

Each run was broken up into periods Δt_{mff}. The RMS for each Δt_{mff} was divided by the mean mass-flow for that period and multiplied by 100 to convert to a percentage.

Figure 6.1a shows the mass-flow fluctuations on the centerline for the power-law calibration. Figure 6.1b shows the mass-flow fluctuations for the same data, but using the Miley calibration instead. In both cases, Δt_{mff} is taken to be 0.01 seconds to again mitigate the effect of the passing expansion wave. Here, the data points are averaged so that only 20 points are shown per run. Thus, each point in the figure represents the average of 20 RMS data points. This allows some sense to be made of the graph. The symbols are different for each run in order to more clearly show the trends of each specific run.

As can be seen, the Miley calibration gives fluctuation levels 2-3 times that of the power-law calibration, in the range of 2-4.5%. The power calibration gives values of

(a) Centerline, power-law calibration (b) Centerline, Miley calibration
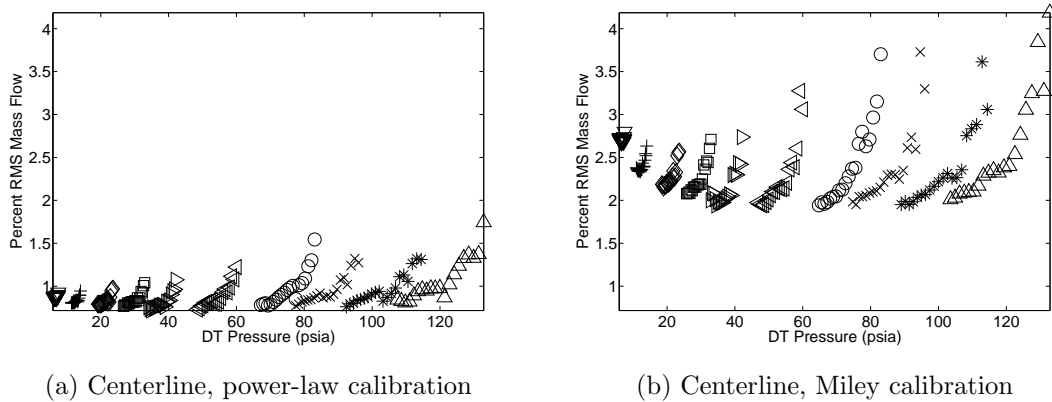
Figure 6.1: Centerline mass-flow fluctuations for both calibrations

0.7-1.7%. The data follow the same general trends in both cases. The fluctuation levels are clearly not solely a function of driver-tube pressure since for each run the fluctuation levels decrease as the run progresses. Also, for pressures below about 30 psia, the minimum fluctuations over the course of a run increases. This is probably due to the decreasing density as the pressure drops. This, in turn, causes the mean mass flow to decrease, resulting in a rise in the normalized mass-flow fluctuations.

In order to ascertain the effect on the mass-flow fluctuations of using a different Δt in the calibration procedure, the fluctuation levels were also calculated using the calibration for a Δt of 0.10 seconds. Figure 6.2 shows fluctuation levels computed with both calibration methods for both Δt's. For the power-law calibration, the difference was negligible as it was on the order of 0.03%. The fluctuations calculated from the Miley calibration, however, proved to be very sensitive to the change in Δt. The fluctuation levels calculated from the two Δt's varied by around 11%. This result underscores the unreliability of the Miley method and made it unusable for any reliable measurements. Instead, the power-law calibration was used for subsequent calculations.

Figure 6.3 shows the power spectra for runs at y_c=0.00 inches and for pressures of 8, 35, 65, 90, and 140 psia. Figure 6.3a is the uncalibrated power spectra of the pre-run voltage and Figure 6.3b is the power spectra of the mass flux calculated over

(a) Power cal., different Δt (b) Miley cal., different Δt
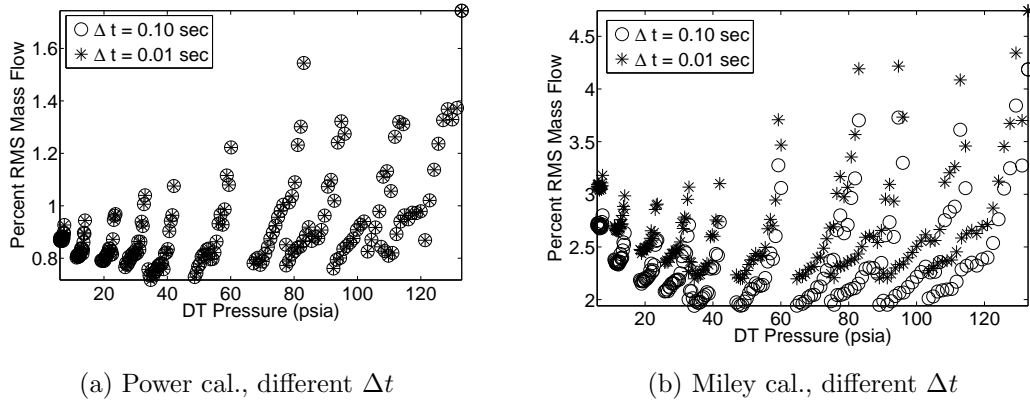
Figure 6.2: Changes in computed fluctuations for different Δt for both calibrations

the time period from 1.0 seconds to 4.5 seconds. The pre-run spectra is uncalibrated since there is no mass flux in the pre-run and thus applying the calibration to the pre-run voltage would give nonsense mass fluxes. It is still useful, however, to see which frequencies are most prevalent in the nominally stagnant air. In all spectrum plots, ρu_{fluc} represents a fluctuating mass flux and ρu_{mean} represents the mean mass flux.

All power spectra were calculated using the "spectrum" command in MatLab. This subroutine calculates the power spectrum based on the specified number of points per FFT window and the sampling frequency at which the data were collected. In all cases, 1000 points were used for each FFT window. This allowed a frequency resolution of 200 Hz.

Calibrated data were used for all but the pre-run spectra. For each 1000 data points, the mean mass flux was calculated. This was subtracted from the instantaneous mass flux and was then normalized by the mean mass flux. The power spectra were then calculated from this quantity. Most of the differences between the pre-run and run spectra are for the higher frequencies. During the runs, the peak frequencies increase from about 65kHz in the pre-run to between 65 and 80kHz during the runs.

In Figure 6.3b, the peak frequency shifts by about 10kHz as pressure increases from 8 psia to 140 psia. There are also several large spikes at around 8, 56, and

(a) Pre-run
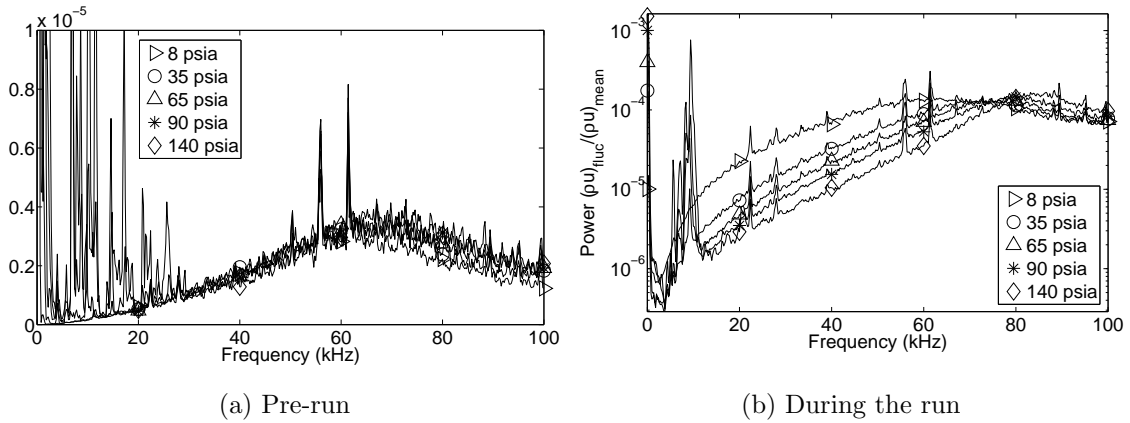
(b) During the run

Figure 6.3: Uncalibrated power spectra at y_c=0.00 inches for pre-run calibrated spectra during the run at several pressures

61 kHz. These are thought to be due to electronic noise since they are present in the pre-run spectra as well. The pre-run spectra also have very large spikes below about 26 kHz. These are most likely due to the observed free convection in the contraction for stagnant air. This explains their absence in Figure 6.3b.

Mass-flow fluctuations were also found for locations 3.00 inches above and below the tunnel centerline in the same manner as for the centerline case. In each instance, the temperature-sensing wire was located 0.18 inches below the mass-flow sensing wire. Figure 6.4 shows the mass-flow fluctuations and power spectra for these wire locations. The fluctuation levels at -3.00 and 3.00 inches appear to be very similar to each other. They are also very close to the fluctuation levels measured on the centerline, both qualitatively and quantitatively. This suggests that fluctuation levels behave in the same manner to a radius of at least 3.00 inches from the centerline.

Additionally, the spectra for these two locations are very similar. The only discernible difference is that the electronic noise peak at 61kHz is larger at y_c=-3.00 inches than at y_c=3.00 inches.

The process of obtaining mass-flow fluctuations for wire locations of -6.00 and 6.00 inches was somewhat more involved. Due to the large diameter of the contraction and the relatively short length of the probe supports (18 inches), only one

(a) Fluctuations at -3.00 inches

(b) Fluctuations at 3.00 inches

(c) Power spectra at -3.00 inches

(d) Power spectra at 3.00 inches
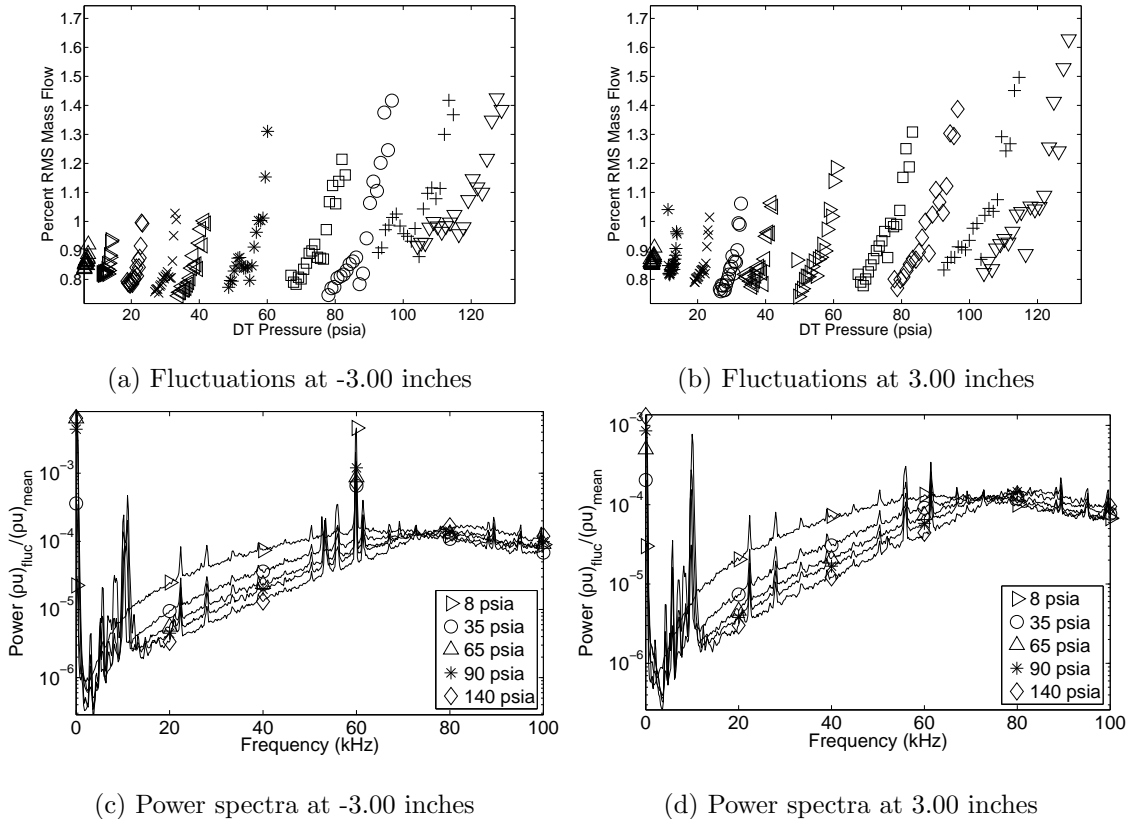
Figure 6.4: Mass-flow fluctuations and calibrated power spectra at y_c=-3.00 and 3.00 inches

wire could be placed at these locations at one time. In order to still be able to use a calibration which took into account the changing temperature, a wire operating in constant current mode was placed at these two locations in order to obtain a temperature-time record. The tunnel was run at initial stagnation pressures of 8, 90, and 140 psia. This series of runs was completed twice in order to check the consistency of the temperature histories at those locations. Figure 6.5 shows the results of these runs. As can be seen, the temperature traces at all three pressures were very consistent both 6.00 inches above and below the centerline. Any differences were only about 1%.

Since the temperature histories were so similar for multiple pressures and trials, temperature histories were also recorded for 25, 35, 45, 65, 105, and 125 psia. These

(a) Temperature vs. time at -6.00 inches   (b) Temperature vs. time at 6.00 inches
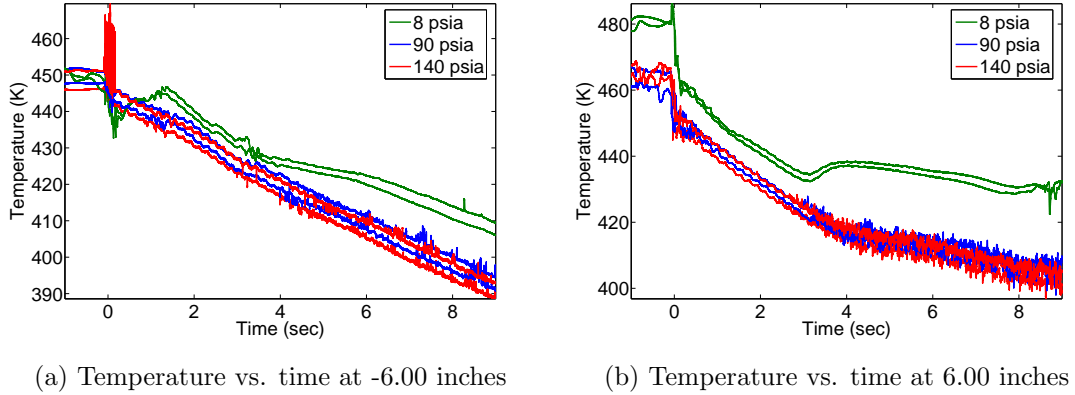
Figure 6.5: Temperature-history check at y_c=-6.00 and 6.00 inches

were then used in the calculation of mass flow fluctuations for wire locations of y_c=-6.00 and 6.00 inches.

Figure 6.6 shows the resultant fluctuation levels at y_c=-6.00 and 6.00 inches. As can be seen, the fluctuations at -6.00 inches are slightly higher overall than those measured on the centerline. They are also, however, significantly lower, by around 20%, than those measured at y_c=6.00 inches. This suggests that somewhere between 3.00 and 6.00 inches above the tunnel centerline, the fluctuation levels become asymmetric.

The power spectra for these locations are, again, very similar. No significant qualitative differences can be seen.

It is interesting to note that there is a qualitative difference in the behavior of the fluctuation levels for 6.00 inches. For other wire locations, the noise levels started off high for a run and then decreased through the end of the run. At 6.00 inches, however, this changed dramatically. The fluctuation levels still started out high and then decreased as the run progressed. However, at some point during each run, the fluctuation levels increased again. By the end of each run, they were typically higher than at the beginning of the run.

In order to understand this behavior, the hot-wire voltage traces were examined. Figure 6.7a highlights the differences between a typical run at -6.00 and 6.00 inches.

(a) Fluctuations at y_c=-6.00 inches

(b) Fluctuations at y_c=6.00 inches

(c) Power spectra at -6.00 inches

(d) Power spectra at 6.00 inches
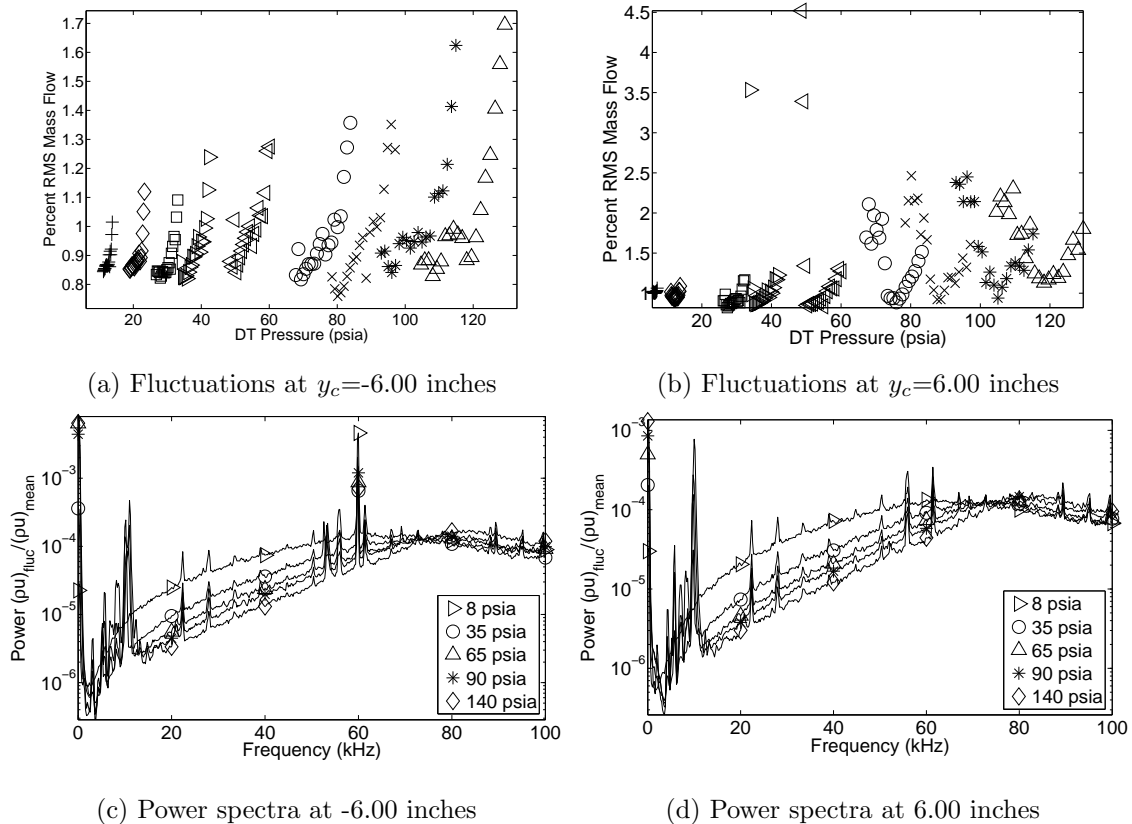
Figure 6.6: Mass-flow fluctuations and calibrated power spectra at y_c=-6.00 and 6.00 inches

In both cases, the initial pressure was 65 psia. Here, only every 100th point is shown. The first 0.25 seconds after the beginning of the run is during the startup of the tunnel. The periodic spikes in the voltage correspond to the passing expansion-wave reflections, which have a period of approximately 200 milliseconds. As can be seen, the oscilloscope trace for a wire location of 6.00 inches drops very suddenly at around 3.9 seconds. After this point, a cursory visual inspection reveals a much higher noise level than for the -6.00 inch case which lacks even the sudden drop in hot-wire voltage. It is thought that this sudden drop in mean voltage and increased noise level is a result of the contraction boundary layer growing on the upper wall of the contraction. This will be discussed in further detail in Chapter 7.

(a) Hot-wire voltage trace
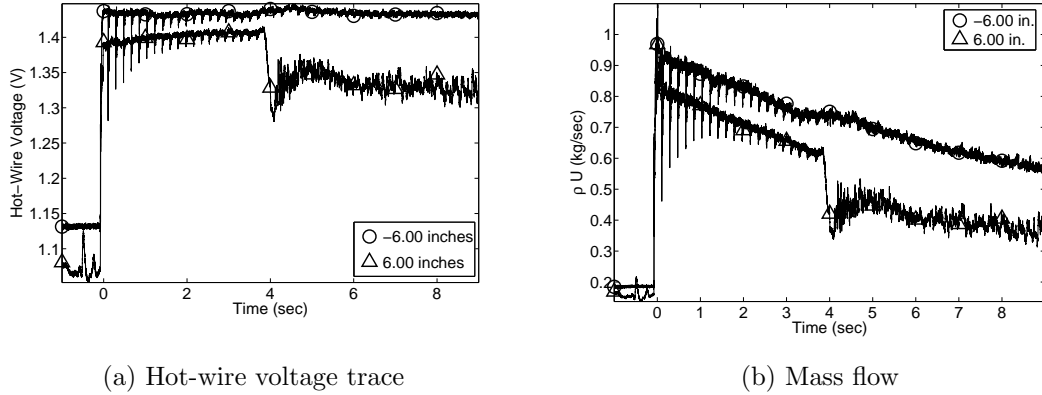
(b) Mass flow

Figure 6.7: Sample hot-wire voltage and corresponding mass flow at y_c=-6.00 and 6.00 inches for initial pressure of 65 psia

In order to present all of the previous data in one simple figure, the average percent-mass-flow-fluctuation level was calculated for each run. Figure 6.8 shows these values plotted against wire location. A line is also included showing the 1% level. As can be seen, for locations of -6.00, -3.00, 0.00, and 3.00 inches, the average fluctuation levels are very similar, ranging from about 0.8% to 1.1%. The fluctuation levels at 6.00 inches are significantly higher, ranging from about 0.95% to nearly 1.7%.

Following Beckwith's criterion of maintaining settling chamber noise levels of less than 1% [17], the fluctuations in the driver tube of the BAM6QT are, on average, marginally too high for centerline distances of -6.00, -3.00, 0.00, and 3.00 inches. During the course of all of these runs, with the possible exception of runs at 8, 15, and 25 psia, the noise level is greater than 1% for a significant portion of the total run.

At y_c=6.00 inches, the noise levels are even higher, with only 15 and 35 psia having an average RMS less than 1%. This further demonstrates the non-uniformity of the driver-tube noise.

Due to differences between the tunnels used by Beckwith and the BAM6QT, it is possible that the observed noise levels are sufficiently low and do not preclude
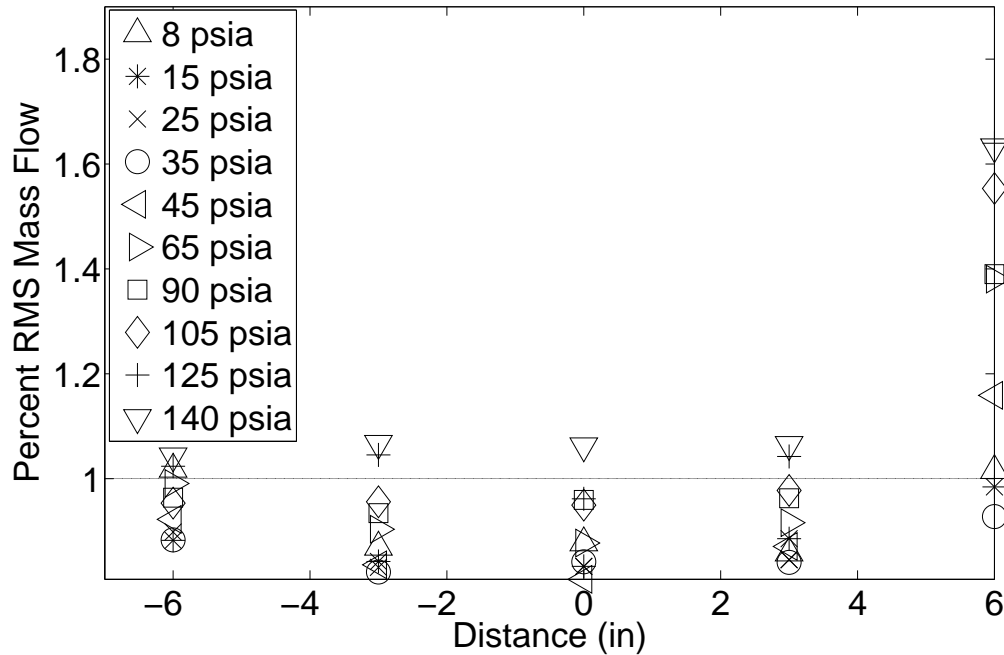
Figure 6.8: Average fluctuation levels for all locations and pressures examined

quiet flow. Beckwith worked with tunnels with much smaller contraction ratios than that of the BAM6QT. For instance, the contraction ratio of the Supersonic Pilot Quiet Tunnel was only about 35, and for the Mach-5 Pilot Tunnel this ratio was about 88 [17]. The BAM6QT has a contraction ratio of about 145. It is conceivable that for a sufficiently large contraction ratio, enough driver-tube noise would be reflected back into the driver tube and not transmitted into the nozzle that driver-tube noise levels of greater than 1% would not affect transition in the nozzle. Since the contraction ratio of the BAM6QT is so much larger than those used by Beckwith, it is possible that noise levels greater than 1% are acceptable for this facility.

Thus, from these results alone, it is difficult to determine whether the driver-tube noise could be adding to nozzle free-stream noise or affecting transition of the nozzle-wall boundary layer. Further characterization of the fluctuations in the contraction is clearly in order.

7. Driver-Tube Boundary Layer

In order to fully understand the nature of the flow present in the contraction, the boundary layer there cannot be neglected. There has not been a great deal of research into boundary-layer growth in Ludwieg tubes. What has been done seems to apply only to small-diameter Ludwieg tubes with run times on the order of tens or hundreds of milliseconds [29–32]. This is not the case for the BAM6QT. Additionally, the reflecting expansion wave makes understanding and prediction of this boundary layer complicated and difficult. Nevertheless, some precursory work was done to try to understand the nature of the contraction-wall boundary-layer.

7.1 Uncalibrated Boundary Layer Measurements

Uncalibrated measurements were made near the upper wall of the contraction. At the time of this investigation, the wire calibration procedure had not been established. Additionally, parameters such as Mach number, temperature, and viscosity, since viscosity is a function of temperature, are not the same in the boundary layer. Thus, the current calibration technique would not hold in the boundary layer.

All runs had an initial stagnation pressure of 45 psia. Runs were made for wall distances of 0.02 to 0.30 inches in 0.025-inch increments. Additional runs were made at 1.02, 2.02, 3.02, 4.02, and 5.02 inches from the upper contraction wall. These distances were chosen because a very simple boundary-layer model predicted a thickness of around 0.1 inches.

As the probe traversed the boundary layer, the mean voltage should have increased until it reached its maximum value in the free stream. Figure 7.1 shows the results of these runs. Here, wall distance is plotted against the mean hot wire voltage, averaged over 0.01 seconds, for 6 different times during the runs. Figure 7.1a shows

the data plotted on linear axes while Figure 7.1b shows the data with y_t plotted on a logarithmic scale in order to better see the data.

(a) Linear axes   (b) y_t log axis
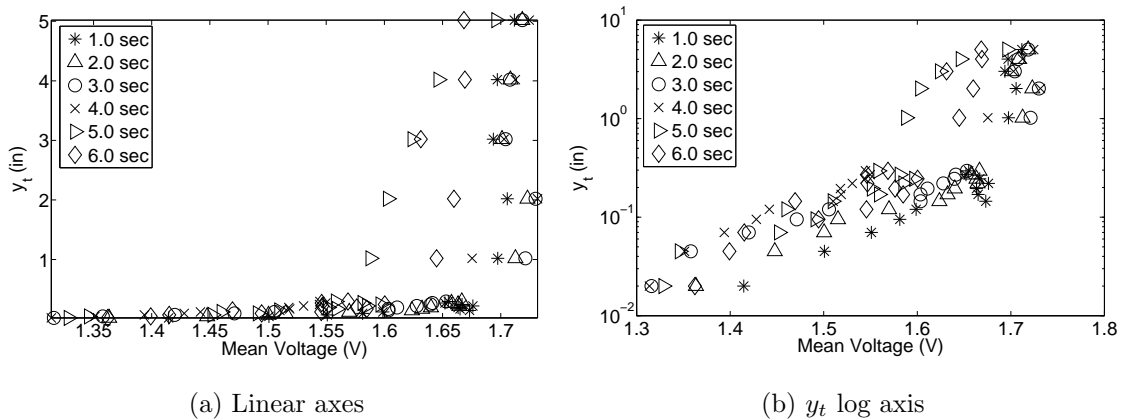
Figure 7.1: Uncalibrated contraction boundary-layer measurements

The figure indicates that the hot-wire voltage generally increased as distance from the wall increased. If the probe were always outside the boundary layer, the mean voltage should be invariant with time. No location ever showed a constant voltage for all times. Instead, each location showed the voltage dropping with time. This would be expected if the probe were in a growing boundary layer. As the boundary layer grew thicker, a specific location would move further from the boundary-layer edge and thus the mass flux would drop. Since this was the observed behavior, it seems that the probe was in a growing boundary layer at all the y_t locations examined.

It is also of note that for $y_t > 1.0$ inches, the mean voltage at 1.0 second is about the same. However, as y_t was increased from 1.02 to 5.02 inches, the total voltage drop over the run decreased markedly. This indicates that for $y_t > 1.0$ inches, the probe was initially outside the boundary layer but then the boundary layer grew to contain those locations. The data indicate that the upper-wall contraction boundary-layer grows to be at least 5 inches thick by 6.0 seconds into a run at 45 psia.

7.2 Qualitative Changes Near the Wall

It was noted that the qualitative nature of the hot-wire oscilloscope traces changed markedly the closer the wire was to the top contraction wall. Figure 7.2 highlights this difference. Three oscilloscope traces are shown. One was for the wire located on the contraction centerline. The others were located at 6.00 and -6.00 inches. All three are for an initial stagnation pressure of 45 psia. Here, only every 100th point is plotted. As usual, the Tektronix TDS7104 oscilloscope was used and was operated in Hi-Res mode with a sampling frequency of 200kS/s.
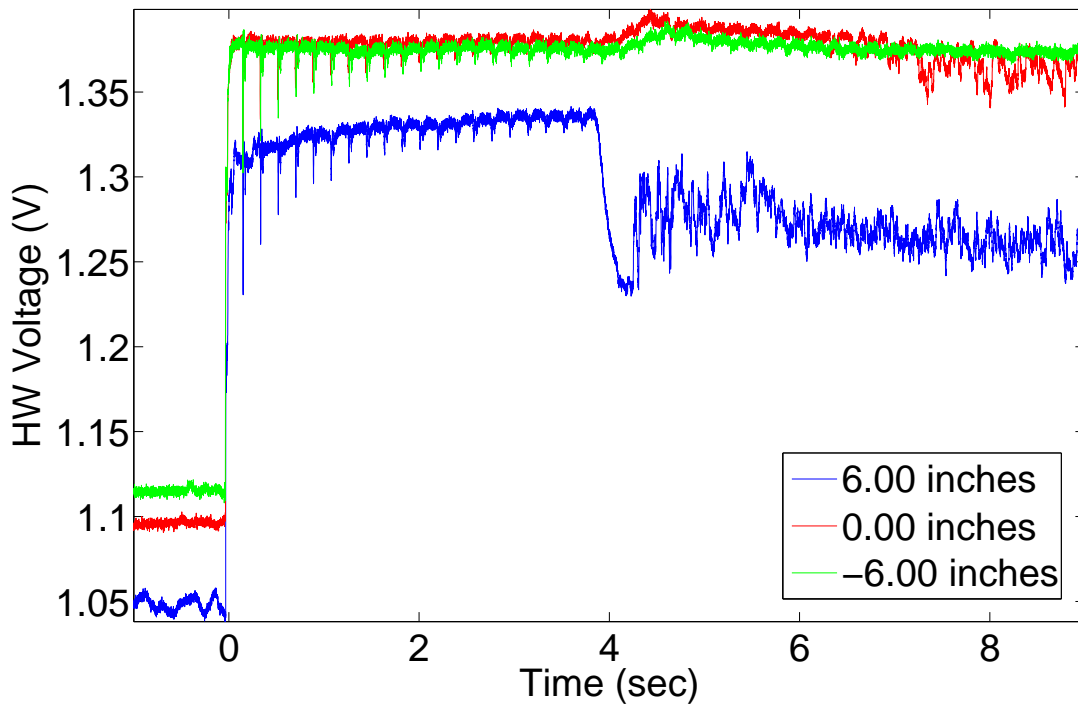
Figure 7.2: Oscilloscope traces at y_c=6.00, 0.00 and -6.00 inches for 45 psia

The trace on the centerline behaves as would be expected. The data recorded between -1.0 and 0.0 seconds corresponds to pre-run data. The large jump in voltage at 0 seconds corresponds to the startup of the tunnel. There is a slight bump in the trace at around 4.5 seconds after which point the voltage begins to decrease until the end of the run. The trace at y_c=-6.00 inches is almost indistinguishable from that of

the centerline. The trace for the wire at y_c=6.00 inches behaves very differently. At about 4.0 seconds, there is a sharp, dramatic decrease in voltage followed by a slight recovery and then high noise until the end of the run. Also, the voltage spikes due to the reflecting expansion wave are no longer discernible. These spikes are periodic and visible at approximately 200 millisecond intervals. This sort of behavior was present in varying degrees for different pressures.

Figure 7.3 shows similar traces for initial stagnation pressures of 8 and 140 psia. The 8 psia centerline trace behaves in a very similar fashion to that of the 45 psia case. The trace for the wire at -6.00 inches is again nearly identical to the centerline trace. The 6.00 inch trace shows significant differences, however. The voltage drop here is not as sharp and begins almost a full second before the 45 psia case. The voltage drop is about the same in these two cases. The axes are scaled differently, however, giving the appearance that it is larger for the 8 psia case. Here, the voltage spikes due to the reflecting expansion wave are still visible after the voltage drop.

(a) 8 psia
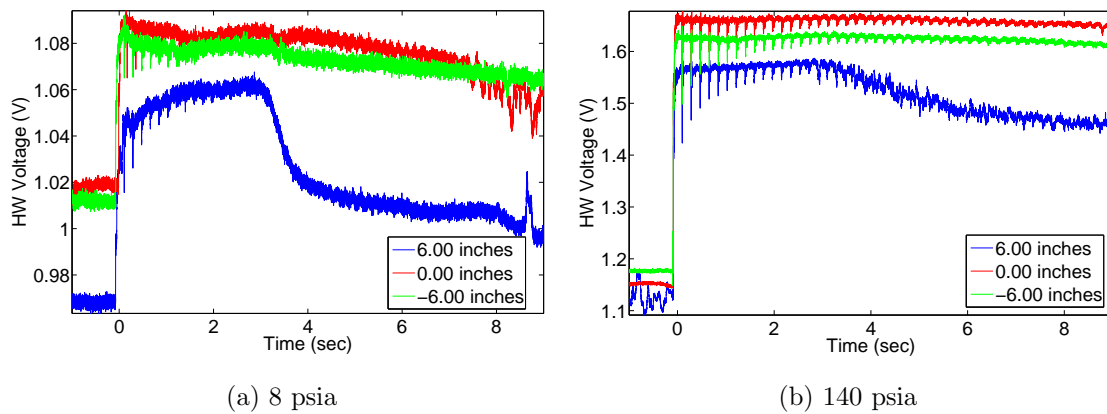
(b) 140 psia

Figure 7.3: Oscilloscope traces at y_c=6.00, 0.00 and -6.00 inches for 8 and 140 psia

The 140 psia case shows the trace on the centerline behaving in similar fashion to those at 8 and 45 psia. The -6.00 inch trace is again very much the same as the centerline case. The 6.00 inch trace behaves much differently than the other two, however. Here, there is no sharp voltage drop. Instead, at about 3 seconds, the signal turns downward and becomes much more noisy. The expansion-wave reflections are

somewhat visible, evidenced by slightly larger voltage spikes about 200 milliseconds apart, though hard to discern from the noise.

It is thought that all this varying behavior is due to the size and state of the boundary layer. For low initial stagnation pressures, such as the 8 psia case, the Reynolds number is very low and thus a thick boundary layer grows. It is possible that the boundary layer grows to include the wire at a location of 6.00 inches, or 2.705 inches from the upper contraction wall. The downward turn in voltage indicates a reduction in mass flow, which would be consistent for a probe in the boundary layer. It also seems realistic that this boundary layer would be laminar. The fact that the expansion-wave reflections can still be discerned from the noise supports this conjecture.

At 45 psia, it also appears that the contraction boundary-layer grows to include the probe when it is 6.00 inches above the centerline even though the higher pressure means a higher Reynolds number and that means a thinner boundary layer. It seems that the boundary layer here is turbulent, evidenced by the lack of expansion-wave reflections in the trace which would probably be lost in the noise of a turbulent boundary layer.

These data corroborate the previous boundary-layer measurements, shown in Figure 7.1a. Both show that the upper contraction-wall boundary-layer as being about 3 inches thick after about 4 seconds into a run at an initial stagnation pressure of 45 psia.

For the 140 psia case, the Reynolds number should be higher than for the other two conditions, giving rise to the thinnest boundary layer. The data seem to support that the boundary layer is indeed thinner. For the trace at 6.00 inches, there is no sharp drop in voltage. Instead, the gradual decrease in mean voltage, the increased signal noise, and the visible expansion-wave reflections suggest that perhaps this location is near the edge of a turbulent boundary layer.

It is significant to note that in all cases, the trace at -6.00 inches does not behave in the same way as the 6.00 inch traces. It is nearly identical to the centerline traces

in all three cases. This implies that it is never in the contraction-wall boundary-layer, even though it is the same distance from the wall as the traces that do appear to be in the boundary layer. Some boundary layer thickening is expected along the top wall because of the previously seen stratification in the driver tube in the pre-run. The stratification makes the initial conditions along the upper wall different than those along the bottom wall. This seems to cause quite a dramatic asymmetry in the boundary layer, if that indeed is the cause of the oscilloscope-trace deformities noted at all pressures 6.00 inches above the centerline.

The data here indicate that a more thorough investigation of the contraction-wall boundary layer is in order. This would help resolve the present uncertainties. It is clear, however, that there are large asymmetries in the flow in the contraction. These asymmetries could easily introduce unwanted disturbances and asymmetries in the nozzle flow further downstream. In order to mitigate these disturbances, they must first be properly understood through more experimental work.

8. Conclusions and Recommendations for Future Work

8.1 Conclusions

The current study has greatly expanded knowledge of the flow in the contraction entrance of the BAM6QT and has also served to highlight areas in which further study is necessary. Several aspects of the contraction were examined in order to characterize the condition of the flow there.

Free convection in the nominally stagnant pre-run air was found to be a source of significant disturbances. This free convection is thought to have been caused by the large temperature gradient that is present over the length of the contraction wall. The gradient led to non-uniform temperatures in the contraction, which induced the free-convection currents. The free-convection effects were measured as noticeable voltage fluctuations in the signals from hot wires operating in both constant current and constant temperature modes.

The temperatures in the contraction above the centerline, during the pre-run and also during the run, were found to be significantly higher than those on the centerline. Before the run, temperatures at y_c=6.00 inches were approximately 40°C higher than on the centerline. After the beginning of the run, the temperatures at that location remained higher than on the centerline, but the difference was much smaller, only about 15°C.

This shows that the contraction wall is actually much hotter than the set point of 160°C, even though the driver-tube walls are near the set point. The contraction overheating appears to be caused by the outer sides of the controlling thermocouples that were left open to the room air. Heat is transferred from their outer sides into the room, making them read a misleading lower temperature. Modifying the contraction

band-heater set-points did lower the observed temperature in the contraction, but the perfect settings were not found to make a uniform 160°C temperature profile.

The observed overheating could also be due excessive heat transfer from the portions of the outer surface of the contraction that are not directly under the band heaters to the room air. Since the controlling thermocouples are affixed to the contraction in such spots on the contraction, this could also cause the controller to read an inaccurate temperature for the contraction.

The ratio of the time-dependent stagnation temperature to the initial stagnation temperature was also computed for a variety of pressures and y_c stations. These data were compared to a simple isentropic theory for the drop in stagnation-temperature ratio. For most of the locations and pressures studied, the data matched the theory well. However, for y_c=6.00 and, in some cases, 3.00 inches, the theory overpredicted the drop. It is thought that the higher pre-run temperatures present near the upper contraction wall are mostly responsible for the deviation from theory. However, the slopes of the curves still often did not match the theoretical slope. This is thought to be due to a thick thermal boundary layer on the upper contraction wall during a run caused by the excessively heated contraction walls and also the stratification of the air in the driver tube prior to a run. This thermal boundary layer appears to be asymmetric due to pre-run stratification of the air in the driver tube and was observed to be much thinner along the bottom wall because it was not observed at y_c=-6.00 or -3.00 inches.

Two methods were used to calibrate hot wires in the incompressible, varying density flow of the contraction. It was found that the established method of Miley and Horstmann is not suitable for the conditions of this experiment. The magnitudes of the computed mass-flow fluctuations were very dependent on the values of the calibration constants. These were found to change significantly depending on the length of time over which each calibration data-point was averaged and a very wide variety of calibration constants caused the calibration data to collapse nicely. This meant that a computed calibration relationship was not unique. To compute

trustworthy mass-flow fluctuations, this is not acceptable. This calibration method was thus deemed unusable for the current study.

Another calibration method was found that avoided the shortcomings of the Miley method. The Nusselt number was related to the wire Reynolds number via a power-law relationship. This calibration shifted only 0.1% when the time period over which calibration data were averaged was changed by two orders of magnitude. It was found that there was only one unique power fit of the data. This led to a stable and trustworthy calibration.

Mass-flow fluctuations were found for many pressures at many y_c locations using this calibration. For locations y_c=-6.00, -3.00, 0.00, and 3.00 inches, the mass-flow fluctuations were generally found to be less than 1.4% for all pressures. At 6.00 inches, however, they were generally found to be less than approximately 2.5%. Thus the levels at all but the 6.00 inch locations are marginally too high according to Beckwith's criterion. At 6.00 inches, they are definitely too high. However, the BAM6QT has now been demonstrated to run quietly to about 95 psia. Thus, driver-tube noise cannot be held responsible for the previous early nozzle-wall boundary-layer transition. It is still possible, however, that the current noise levels will preclude quiet flow to higher stagnation pressures. The fluctuation levels in the driver tube cannot yet be considered low enough to not threaten future quiet-flow development. Additional work is clearly in order.

A precursory examination of the contraction-entrance boundary-layer was also undertaken. Initial measurements at 45 psia showed a boundary layer thickness of at least 5 inches by the end of a run at an initial stagnation pressure of 45 psia. This preliminary data were substantiated by examining a qualitative change between a hot-wire voltage trace on the centerline and one at $y_c = 6.00$ inches. The behavior of the traces shows what may be a thick, laminar boundary layer at 8 psia, a thinner turbulent boundary layer at 45 psia, and an even thinner turbulent boundary layer at 140 psia. None of this was evident for hot-wire traces taken at y_c=-6.00 inches,

suggesting an asymmetric contraction-wall boundary layer. Further work is clearly in order in this area as well.

8.2 Recommendations for Future Work

Although much progress has been made toward characterizing the conditions and flow at the driver tube exit, there are still a number of unresolved issues that should be addressed.

Free convection studies should continue in the contraction as they seem to be a source of significant fluctuations. Since the hardware necessary to instrument most of the area below the centerline of the contraction was not in place until late in the current effort, this area of the contraction should be studied to determine and characterize any free-convection effects.

A plug should also be inserted into the nozzle throat and similar measurements made. This would show whether or not cooler air from downstream in the nozzle feeds upstream into the contraction during the pre-run and causes free convection. Since a plug cannot remain in the nozzle throat if the tunnel is to be run, the throat and possibly sections of the nozzle downstream of the throat, should be heated. This could alleviate cooler air feeding upstream during the pre-run.

Additionally, further refinement of the general temperature profile in the contraction should be undertaken, especially below the centerline. The contraction and driver-tube temperature settings should also be studied. They should be varied systematically to determine the optimal settings to achieve maximum temperature uniformity. Nitrogen liquefaction in the nozzle exit must also be taken into consideration. The driver tube and contraction temperatures must be set to avoid this effect.

It would be good to make similar measurements of free convection and temperature upstream, towards the center of the driver tube, to avoid contraction-end temperature gradient effects. However, the code-stamped driver tube has no access

ports to enable such measurements. A new pipe section with instrumentation ports would have to be built and inserted between the flanges of the existing pipe to enable such measurements.

The hot-wire calibration technique should be further studied. Another wire should be calibrated and used to determine mass-flow fluctuations at the same conditions as in the present study. Also, a wire with a smaller aspect ratio should be calibrated and used to determine fluctuation levels to ensure that these parameters do not affect the measured levels.

Since current results show the driver-tube noise as being moderately too high by Beckwith's criterion, mitigation of fluctuation levels via hardware modification should be considered. Beckwith used relatively cheap and easy-to-use acoustic baffles, porous plates, and steel wool. It is unclear whether these are suitable for a short-run-time Ludwieg tube, but this avenue should be explored nonetheless.

To gain a better understanding of the propagation of driver-tube noise into the nozzle, a controlled disturbance could also be introduced into the upstream end of the driver tube. This could be accomplished by installing a speaker attached to the output of a signal generator. This way, a controlled disturbance of known spectral content could be introduced at the upstream end of the driver tube and measured both in the contraction entrance and in the nozzle exit. The transmitted power of the signal could then be computed. This would give a much clearer understanding of the level of acceptable disturbances in the driver tube of the BAM6QT.

Additional understanding of the growth, development, and behavior of the contraction boundary-layer can be accomplished in a number of ways. Further hot-wire measurements should be made closer to both the upper and lower contraction walls. Additionally, glue-on hot-film-probes can be affixed to the inside of the contraction walls. These would show whether the boundary layer is laminar or turbulent. Additionally, transition of the boundary layer could be studied. This would be of great help in determining if the bleed suction is sufficient to entirely remove the contraction boundary layer and its associated disturbances.

An understanding of the boundary-layer growth should then be incorporated into the hot-wire calibration. As the displacement thickness grows, the Mach number in the contraction diverges from the inviscid, isentropic value. This is not accounted for in the current calibration scheme. Incorporating this changing Mach number into the calibration would enable a more accurate calibration to be found and used for subsequent measurements.

Although a great deal has been learned about the state of the flow in the contraction, the work there should continue. It is not clear that the present state of the contraction is such that it will allow quiet flow to be achieved to the design point of the tunnel. Only with careful further study and possible modifications can the contraction and driver tube be determined to be operating within acceptable parameters.

LIST OF REFERENCES

LIST OF REFERENCES

[1] Steven P. Schneider. Effects of high-speed tunnel noise on laminar-turbulent transition. *Journal of Spacecraft and Rockets*, 38(3):323–333, May-June 2001.

[2] Helen L. Reed, Roger Kimmel, Steven Schneider, and Daniel Arnal. Drag prediction and transition in hypersonic flow. Paper 97-1818, AIAA, June 1997.

[3] S.R. Pate and C.J. Schueler. Radiated aerodynamic noise effects on boundary-layer transition in supersonic and hypersonic wind tunnels. *AIAA Journal*, 7(3):450–457, 1969.

[4] Steven P. Schneider. Fabrication and testing of the Purdue Mach-6 quiet-flow Ludwieg tube. Paper 2000-0295, AIAA, January 2000.

[5] Steven P. Schneider. Design and fabrication of a 9.5-inch Mach-6 quiet-flow Ludwieg Tube. Paper 98-2511, AIAA, June 1998.

[6] Craig R. Skoch. Final assembly and initial testing of the Purdue Mach-6 quiet-flow Ludwieg tube. Master's thesis, Purdue University, December 2001.

[7] Craig R. Skoch, Steven P. Schneider, and Matthew P. Borg. Disturbances from shock/boundary layer interactions affecting upstream hypersonic flow. Paper 2005-4897, AIAA, June 2005.

[8] Steven P. Schneider, May 2005. Private communication.

[9] Steven P. Schneider and Craig Skoch. Mean flow and noise measurements in the Purdue Mach-6 quiet-flow Ludwieg tube. Paper 2001-2778, AIAA, June 2001.

[10] Steven P. Schneider, Shin Matsumura, Shann Rufer, Craig Skoch, and Erick Swanson. Progress in the operation of the Boeing/AFOSR Mach-6 quiet tunnel. Paper 2002-3033, AIAA, June 2002.

[11] Steven P. Schneider, Craig Skoch, Shann Rufer, Shin Matsumura, and Erick Swanson. Transition research in the Boeing/AFOSR Mach-6 quiet tunnel. Paper 2002-0302, AIAA, January 2002.

[12] Steven P. Schneider, Craig Skoch, Shann Rufer, and Erick Swanson. Hypersonic transition research in the Boeing/AFOSR Mach-6 quiet tunnel. Paper 2003-3450, AIAA, June 2003.

[13] Steven P. Schneider, Craig Skoch, Shann Rufer, Erick Swanson, and Matthew Borg. Laminar-turbulent transition research in the Boeing/AFOSR Mach-6 quiet tunnel. Paper 2005-0888, AIAA, January 2005.

[14] Ivan E. Beckwith, F.-J. Chen, and T.R. Creel Jr. Design requirements for the NASA Langley supersonic low-disturbance wind tunnel. Paper 86-0763, AIAA, March 1986.

[15] Ivan E. Beckwith and E. Wayne Martin. Propagation of settling chamber noise in supersonic wind tunnels. Presented at the 57th semiannual meeting of the Supsonic Tunnel Association, March 1982.

[16] John Laufer and Jack E. Marte. Results and a critical discussion of transition-Reynolds-number measurements on insulated cones and flat plates in supersonic wind tunnels. Technical Report 20-96, Jet Propulsion Laboratory, November 1956.

[17] Ivan E. Beckwith. Comments on settling chamber design for quiet, blowdown wind tunnels. NASA Technical Memorandum 81948, March 1981.

[18] Ivan E. Beckwith and P. Calvin Stainback. Transition research and prospects for a Mach 3 to 7 quiet tunnel. Langley Working Paper 1064, July 1972.

[19] P.C. Stainback and K.A. Nagabushana. Review of hot-wire anemometry techniques and the range of their applicability for various flows. *American Society of Mechanical Engineers, Fluids Engineering Division FED, Thermal Anemometry 1993*, v 167:93–133, 1993. Information for this thesis was taken from an extended version of this paper of the same title in an electonic version of the Journal of Fluids Engineering.

[20] E.F. Spina and C.B. McGinley. Constant-temperature anemometry in hypersonic flow: critical issues and sample results. *Experiments in Fluids*, 17:365–374, 1994.

[21] Steven P. Schneider, Craig Skoch, Shann Rufer, Erick Swanson, and Matthew Borg. Bypass transition on the nozzle wall of the Boeing/AFOSR Mach-6 quiet tunnel. Paper 2004-0250, AIAA, January 2004.

[22] L.M. Fingerson and Peter Freymuth. *Fluid Mechanics Measurements*, chapter 3, Thermal Anemometers. Taylor & Francis, 1996.

[23] Alan Pope and Kennith L. Goin. *High-speed wind tunnel testing*. Robert E. Krieger Publishing Company, 1965.

[24] Steven P. Schneider, Steven H. Collicott, J. D. Schmisseur, Dale Ladoon, Laura A. Randall, Scott E. Munro, and T. R. Salyer. Laminar-turbulent transition research in the Purdue Mach-4 Quiet-Flow Ludwieg Tube. Paper 96-2191, AIAA, June 1996.

[25] Shann Rufer, October 2005. Private communication.

[26] Frank M. White. *Viscous Fluid Flow*, pages 27–31. McGraw-Hill, 2nd edition. Madison, WI, 1991.

[27] S. J. Miley and Dr. Ing. K. H. Horstmann. Data report of flight and wind-tunnel investigations of Tollmien-Schlichting waves on an aircraft wing. Technical Report IB 129-91/18, Institut fur Entwurfsaerodynamik, DLR, December 1991.

[28] Eds. D. Fisher, K.H. Horstmann, and H. Riedle. Flight test measurement techniques for laminar flow. AGARDograph 300, Research and Technology Organisation, October 2003.

[29] E. Becker. Unsteady boundary layers behind compression shocks and expansion waves. *Progress in Aeronautical Sciences*, 1:104–173, 1961. Translated from German to English by Associated Technical Services, Glen Ridge, NJ, 1969.

[30] Chung-Hwan Chun and Taesung Ha. Investigation of the unsteady boundary layer development in a Ludwieg tube. Unpublished report from the Department of Mechanical Engineering, Pohang University of Science and Technology, Republic of Korea. Emailed on 2 June, 2005 by Ch.-H. Chun.

[31] Eckart Piltz. Boundary-layer effects on pressure variations in Ludwieg tubes. *AIAA Journal*, 10(8):1095–1097, 1972.

[32] David A. Russell, Gerald S. Knoke, and John C. Wai. Uniformity of Ludwieg tube flows. From Modern Developments in Shock Tube Research 10th Annual International Shock Tube Symposium, Kyoto, 1975. p. 244-251.